

Structure-Based Design, Optimization and Development of [18F]LU13, a novel radioligand for CB2R Imaging in the Brain with PET

Gündel, D.; Deuther-Conrad, W.; Ueberham, L.; Kaur, S.; Otikova, E.; Teodoro, R.; Lai, T. H.; Clauß, O.; Scheunemann, M.; Bormans, G.; Bachmann, M.; Kopka, K.; Brust, P.; Moldovan, R.-P.;

Originally published:

June 2022

Journal of Medicinal Chemistry 65(2022)13, 9034-9049

DOI: <https://doi.org/10.1021/acs.jmedchem.2c00256>

Perma-Link to Publication Repository of HZDR:

<https://www.hzdr.de/publications/Publ-33987>

Release of the secondary publication
on the basis of the German Copyright Law § 38 Section 4.

Structure-Based Design, Optimization and Development of [¹⁸F]LU13, a Novel Radioligand for Cannabinoid Receptor Type 2 (CB2R) Imaging in the Brain with PET

Daniel Gündel¹, Winnie Deuther-Conrad¹, Lea Ueberham¹, Sarandeep Kaur¹, Elina Otikova¹, Rodrigo Teodoro¹, Magali Toussaint¹, Thu Hang Lai^{1, 5}, Oliver Clauß¹, Matthias Scheunemann¹, Guy Bormans², Michael Bachmann¹, Klaus Kopka^{1,4}, Peter Brust^{1,3} and Rareş-Petru Moldovan^{1,*}

¹ Helmholtz-Zentrum Dresden-Rossendorf (HZDR), Institute of Radiopharmaceutical Cancer Research, Department of Neuroradiopharmaceuticals, Research site Leipzig, 04318 Leipzig, Germany

² Radiopharmaceutical Research, Department of Pharmaceutical and Pharmacological Sciences, KU Leuven, BE-3000 Leuven, Belgium

³ The Lübeck Institute of Experimental Dermatology, University Medical Center Schleswig-Holstein, 23562 Lübeck, Germany

⁴ Faculty of Chemistry and Food Chemistry, School of Science, TU Dresden, 01069 Dresden, Germany

⁵ ROTOP Pharmaka GmbH, Department of Research and Development, 01069 Dresden, Germany

* Correspondence: Rareş-Petru Moldovan (r.moldovan@hzdr.de, Tel.: +49-3412341794634)

KEYWORDS. *cannabinoid receptor type 2; naphthylid-2-one; binding affinity; radiochemistry; fluorine-18 labeling; brain; positron-emission tomography.*

ABSTRACT: The cannabinoid receptor type 2 (CB2R) is an attractive target for the diagnosis and therapy of neurodegenerative diseases and cancer. In this study, we aimed at the development of a novel ¹⁸F-labeled radioligand starting from the structure of the known naphthylid-2-one CB2R ligands. Compound **28 (LU13)** was identified with the highest binding affinity and selectivity versus CB1R (CB2R*K_i* = 0.6 nM; CB1R*K_i*/CB2R*K_i* > 1000) and was selected for radiolabeling with fluorine-18 and biological characterization. The new radioligand [¹⁸F]LU13 showed high CB2R affinity in vitro as well as high metabolic stability in vivo. PET imaging with [¹⁸F]LU13 in a rat model of vector-based/related hCB2R overexpression in the striatum revealed a high signal-to-background ratio. Thus, [¹⁸F]LU13 is a novel and highly promising PET radioligand for the imaging of upregulated CB2R expression under pathological conditions in the brain.

INTRODUCTION

The hemp plant *Cannabis sativa* has been used as medicine for analgesic, anticonvulsive, and antiphlogistic applications for centuries.¹ It is exerting its pharmacological activity through the bioactive natural compounds called cannabinoids by modulating the endogenous cannabinoid system (ECS).² The ECS is a neuromodulatory system which consists of the cannabinoid receptors, the endogenous ligands *N*-arachidonylethanolamine (AEA) and 2-arachidonoylglycerol (2-AG), as well as the enzymes responsible for endocannabinoid biosynthesis, cellular uptake and metabolism.²⁻⁴ Two types of cannabinoid receptors have been well characterized so far, cannabinoid receptor type 1 (CB1R) and cannabinoid receptor type 2 (CB2R).^{5,6} Both CB1R and CB2R are members of the rhodopsin-like family of G-protein coupled receptors (GPCRs), which are characterized by a seven-transmembrane helical structure, sharing 44% overall identity and 68% similarity for the transmembrane domains.⁷ CB1R is mainly expressed in the central nervous system (CNS), in neurons and glial cells, where it modulates several functions such as memory, cognition, emotion and pain control.⁸ In peripheral tissues (lung, kidney, and liver) CB1R modulates metabolism and energy balance.⁹ On the other hand, CB2R are mainly associated with the immune system, in particular macrophages, B- and T- cells.^{6,10} In the brain, the CB2R is physiologically expressed at a very low level, mainly by the microglial cells.^{11,12} The activation of CB2R on microglial cells has been shown to inhibit the release of proinflammatory cytokines and to induce the release of anti-inflammatory cytokines.¹³ Therefore, it is assumed that the ECS plays a crucial role in microglial-derived neuroinflammation through the activation of CB2R, regulating distinct components of the brain inflammatory response, including microglial cell proliferation, migration, and differentiation into M1 or M2 phenotypes.¹³⁻¹⁷ The overexpression of the CB2R in the brain is related to inflammatory processes associated with neurodegenerative diseases such as Alzheimer's disease, Parkinson's disease and Huntington's disease, as well as cancer.^{14,18-31} Especially the treatment with CB2R agonists represents a promising approach for the treatment of CNS disorders.³² The detection of neurological diseases at an early stage by a sensitive and non-invasive method like positron emission tomography (PET) might support an efficient and personalized therapy. The imaging of the CB2R in the brain with PET takes advantage of the very low level of expression of CB2R in healthy brain complemented by overexpression in pathological conditions and thus, presumably resulting in a high signal-to-background ratio. Up to date, none of the reported CB2R PET radioligands proved to be suitable for routine clinical use.³³⁻³⁵ The development of radioligands for PET imaging of the CB2R in the brain is challenged by the generally inadequate pharmacological properties of the CB2R ligands (lipophilicity, metabolic stability, pharmacokinetic) and by the lack of a suitable animal model for the preclinical investigations.³³⁻³⁵

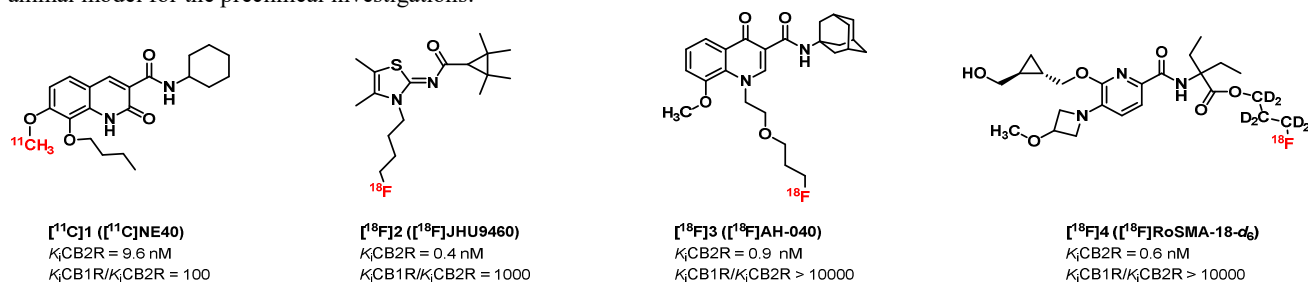


Figure 1. Chemical structures of representative CB2R radioligands

A number of ¹¹C and ¹⁸F-labeled CB2R radioligands have been developed to date.³³⁻³⁵ The most representative ones are shown in Figure 1. Early work by Evens and co-workers led to the development of [¹¹C]NE40 ([¹¹C]1)^{36,37}, which is the only CB2R radioligand that was tested in human subjects.³⁸ Moldovan and co-workers reported the development and preliminary evaluation in vivo of [¹⁸F]JHU94620 ([¹⁸F]2)^{39,40} providing evidence for the importance of CB2R imaging under neuroinflammation with PET. The group of Ametamey and Mu developed an impressive series of ¹¹C- and ¹⁸F-labeled 4-oxo-quinolines out of which [¹⁸F]AH-040 ([¹⁸F]3)⁴¹⁻⁴³ is shown in Figure 1. More recently, Ametamey and co-workers developed an ¹⁸F-labeled pyridine-based radioligand (compound [¹⁸F]4, [¹⁸F]RoSMA-18-d6, Figure 1)^{44,45} with promising imaging properties. However, the imaging of the CB2R in the brain is still challenged by the limitations of these radioligands like unfavorable pharmacokinetics, high non-specific binding, low brain uptake or low metabolic stability and the presence of brain-penetrant radiometabolites. Recently, we reported the development and preliminary evaluation of [¹⁸F]LU14 ([¹⁸F]5, Figure 2) and provided evidence for the brain-penetrant nature of this scaffold.⁴⁶ Compound [¹⁸F]LU14 was developed based on a library of naphthyridine-2-one-carboxamides developed by Lucchesi and co-workers and further investigated by Pascali and co-workers.^{47,48} Thus, in the present work we report our efforts to develop a novel ¹⁸F-labeled radioligand with improved binding affinity and metabolic stability by systematic modifying the structure of the literature known naphthyrid-2-one based CB2R ligands (compounds **5**, **10** and **16**)^{46,47,49}. A schematic overview of our structure-based optimization program is shown in Figure 2, highlighting the three positions at which modifications are performed: *i*) the carboxamide subunit, *ii*) the *N*-alkyl chain and *iii*) the C-6 position. Previous work reported by Lucchesi⁴⁷ and by us⁴⁶ proved the superior binding affinity of the ligands bearing a *cis*-configuration of the 4-methyl cyclohexylamine. Therefore, in the present work we focus on evaluating the novel compounds in diastereomerically pure form. Moreover, we attempt its replacement by different substituents and evaluate the impact on the binding affinity towards the CB2R. The modifications performed at the *N*-alkyl chain are responsible for the improved metabolic stability, and thus, the introduction of the metabolically more stable fluoroaryl subunits are favored.⁵⁰ Alternatively, the deuteration of fluoroalkyl residues was shown to considerably improve the metabolic stability for a number of PET radioligands.⁵¹ In our efforts to increase the binding affinity of our ligands, we also investigated the influence of the C-6 substitution. The most promising candidate was selected for ¹⁸F-labeling and biological evaluation. Typically, the spleen serves as a reference organ for the evaluation of a novel CB2R radioligand due to the high expression density of the CB2R under physiological conditions. In this work, we use a well-established rat model carrying an adeno-associated viral (AAV2/7) vector expressing hCB2R(D80N) at high densities in a striatal region.^{36,52,53} Our strategy is providing important information regarding the brain up-2

take of the novel radioligand as well as its ability to image the hCB2R within the brain.

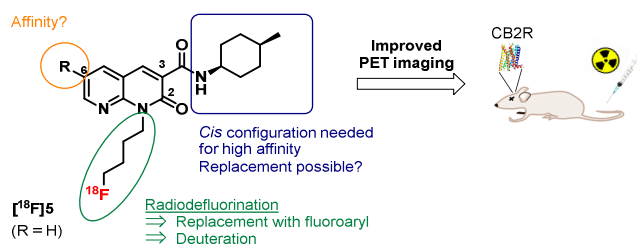
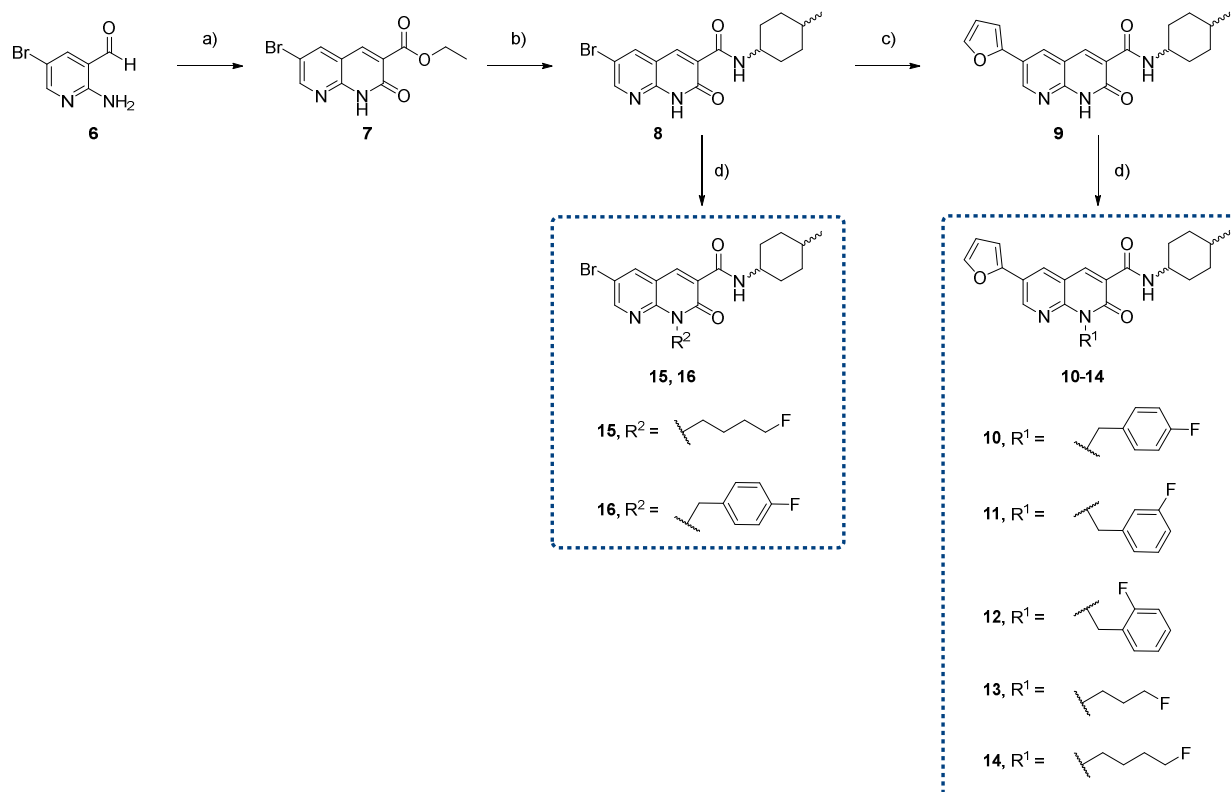


Figure 2. Design strategy of target compounds

RESULTS AND DISCUSSION

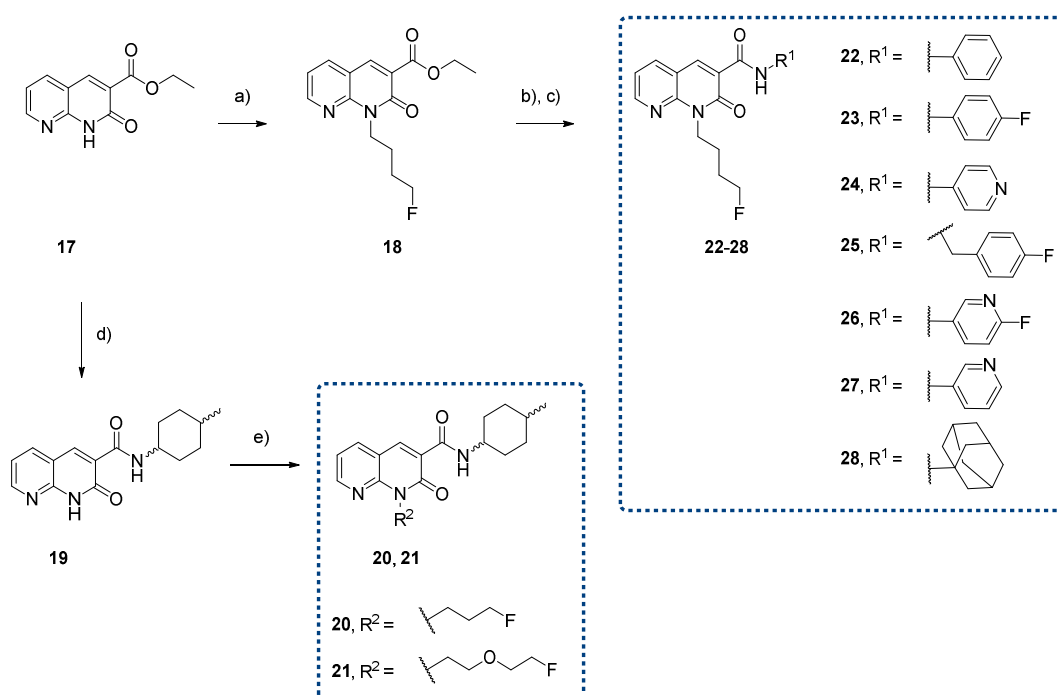
Chemistry. The synthetic routes of the key intermediates and target compounds are outlined in Scheme 1 and 2.^{46, 47} The synthesis of derivatives bearing bromide or furan at the naphthyridine-2-one-carboxamides position-6 is shown in Scheme 1. The synthesis starts from the commercially available 2-aminonicotinaldehyde which in the first step is brominated at the C-5 position to give compound **6**. Afterwards, Knoevenagel condensation is performed followed by thermal coupling with 4-methylcyclohexylamine to produce the key intermediate **8**. Next, compound **8** was alkylated either at the N-1 position to give target compounds **15** and **16** or subject to a Stille reaction to give the 6-furan intermediate **9**. Finally, compounds **10-14** were synthesized by alkylation at the N-1 position of compound **9** as described above. For the biological studies, the *cis*- and *trans*- isomers of 4-methylcyclohexylamine mixtures were separated by flash chromatography on silica.

Scheme 1. Synthesis of Position-6 Substituted Naphthyridine-2-one-carboxamide Target Compounds^a



^aReagents and conditions: a) diethyl malonate, piperidine, EtOH, reflux, 20 h; b) 4-methylcyclohexylamine, 150 °C, 18 h; c) 2-(tributylstannyl)furan, PdCl₂(PPh₃)₂, DMF, 90 °C, 3 h; d) R¹X/R²X, Cs₂CO₃, DMF, 50 °C, 16 h (X = halogen).

Scheme 2. Synthesis of Naphthyridine-2-one-carboxamide Target Compounds Unsubstituted at Position-6^a



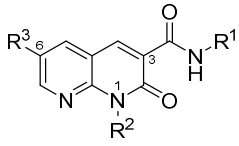
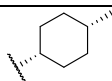
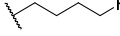
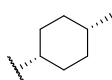
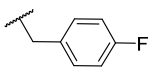
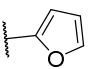
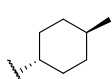
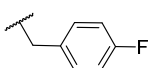
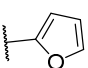
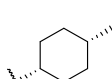
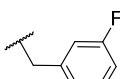
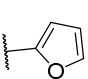
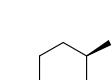
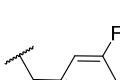
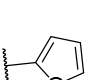
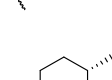
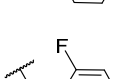

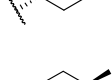
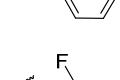

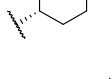
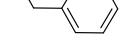
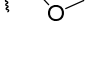
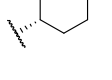
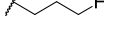
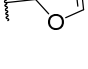
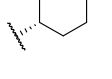
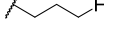
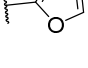
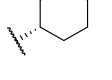

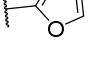
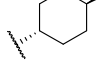
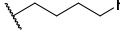
^aReagents and conditions: a) 1-bromo-4-fluorobutane, K₂CO₃, DMF, 90 °C, 19 h; b) LiOH·H₂O, THF/MeOH/H₂O (2:1:1, v/v/v), 60 °C, 2.5 h; c) R¹NH₂, BOP, NEt₃, CH₂Cl₂, 16 h, rt; d) 4-methylcyclohexylamine, 150 °C, 18 h; e) R²X, Cs₂CO₃, DMF, 50 °C, 16 h. BOP = [(1*H*-benzo[*d*][1-3]triazol-1-yl)oxy]tris(dimethylamino)phosphonium hexafluorophosphate(V).

In Scheme 2, the detailed synthesis of naphthyridine-2-one-carboxamides ligands unsubstituted at C-6 position and modified at either *N*-1 position or the carboxamide subunit is shown. Derivatives **22-28**, modified at the carboxamide subunit were synthesized starting with the naphthyridine-2-one-carboxylate **17**. In the first step, **17** is *N*-alkylated under alkaline reaction conditions followed by ester hydrolysis and subsequent BOP mediated amide coupling with various primary amines. The synthesis of the *N*-functionalized derivatives **20** and **21**, starts with the thermal-induced condensation of **17** with 4-methylcyclohexylamine followed by *N*-alkylation with alkyl halogenates in the presence of a base.

In Vitro Binding Assay. The main purpose of our SAR study was to develop an ¹⁸F-labeled analogue of **5** with an increased binding affinity towards CB2R. Although the overexpression of the CB2R was demonstrated for a number of neurological diseases, the CB2R are expressed at a very low level in the healthy brain. In order to detect neurological changes at an early stage, we aimed at the development of a CB2R ligand with subnanomolar affinity. Moreover, due to the high level of expression of the CB1R in the brain, a high selectivity (*K*_iCB1R/*K*_iCB2R > 500) was strived. The binding affinity of the herein described naphthyridine-2-one-carboxamides towards the hCB1R and hCB2R was evaluated by an in-house well-established protocol (Table 1).³⁹ As shown in Table 1, the new derivatives were designed by modifying the carboxamide moiety (R¹), the *N*-alkyl chain (R²) and the C-6 position (R³). Due to the insufficient binding affinity of compound **5** (CB2R*K*_i = 6 nM)⁴⁶ we switched our attention to compound *cis*-**10** bearing the furan moiety at position C-6 and 4-fluorophenyl at the *N*-1 position and with previously described CB2R binding affinity of 0.27 nM.⁴⁷ However, with our protocol, compound *cis*-**10** showed a binding affinity of 5 nM towards CB2R. Furthermore, we evaluated the 3- and 2-fluorobenzyl regioisomers of compound **10** (compounds **11** and **12**, Table 1) and determined only a slightly higher affinity for the 3-fluorobenzyl derivative, whereas a loss of affinity was observed for the 2-fluorobenzyl analogue. The evaluation of the *N*-fluoroalkyl derivatives (**13-14**) revealed a high affinity for the fluorobutyl-substituted compound *cis*-**14** and a decreased affinity for the fluoropropyl analogue *cis*-**13**. Next, we evaluated the affinity of the C-6 brominated compounds bearing either 4-fluorobutyl or 4-fluorobenzyl residues at *N*-1 position and determined bindings affinities of 4.8 nM and 1.7 nM for **15** and **16**, respectively. To conclude this first series of compounds bearing a substituent at the C-6 position (compounds **10-16**), we were not able to obtain derivatives with a sub-nanomolar affinity towards CB2R. Moreover, these compounds possess a relatively high molecular weight (MW > 450) and higher lipophilicity with cLogP in the range of 4.5-5 compared to [¹⁸F]**5** which has a cLogP of 3.5 and an experimentally determined logD_{7.4} of 3.15.⁴⁶ Keeping in mind the favorable range of logD for brain-targeting pharmaceuticals (logD, 1-4)^{54, 55} we redirected our attention for the C-6 non-substituted derivatives and extended the series of derivatives mainly by modifying the substituent at the carboxamide subunit. The introduction of an aryl moiety at this position had a strong impact on the binding affinity of the resulting compounds and each of the (fluoro)phenyl and (fluoro)pyridyl derivatives **22-27** showed CB2R*K*_is in the micromolar range. However, compound **28** (**LU13**) bearing the adamantane moiety at the carboxamide subunit possesses a remarkably high binding affinity of 0.6 nM towards the CB2R. We also investigated the 4-fluorobenzyl and 2-4

(2-fluoroethoxy)ethyl (**29** and **30** respectively, synthesis not shown in Scheme 2, see Experimental section), but they proved to be slightly less affine. In general, for the whole series of compounds a higher CB2R affinity was determined for the *cis*- compared to *trans*-derivatives and a constantly low CB1R affinity was determined for all the herein investigated derivatives, which is in agreement with early reports of Lucchesi⁴⁷ and Manera⁴⁹. Our study led to the development of the adamantane substituted **LU13** with a subnanomolar affinity towards CB2R, high selectivity against CB1R, moderate molecular weight and lipophilicity (cLogP = 3.6), as a new candidate for a CB2R targeting radioligand development.

Table 1. Binding Affinities of 5 and the New Derivatives ^a

						
Compound	R ¹	R ²	R ³	CB2R <i>K</i> _i nM	CB1R <i>K</i> _i nM	CB1R/CB2R
5			H	6 ^b (1.4 ^c)	> 1,000	> 167
<i>cis</i> - 10				5.0 (0.27 ^c)	915	> 183
<i>trans</i> - 10				86	NA	NA
<i>cis</i> - 11				2.9	> 10,000	> 1,000
<i>trans</i> - 11				5000	NA	NA
<i>cis</i> - 12				65	> 10,000	> 153
<i>trans</i> - 12				> 10,000	NA	NA
<i>cis</i> - 13				28	> 1,000	NA
<i>trans</i> - 13				6,800	NA	NA
<i>cis</i> - 14				3.3	> 1,000	> 303
<i>trans</i> - 14				49	NA	NA
15			Br	4.8	> 1,000	NA

16			Br	1.7	> 155	91
<i>cis</i> -20			H	115	NA	NA
<i>trans</i> -20			H	4,600	NA	NA
<i>cis</i> -21			H	13	> 10,000	> 714
<i>trans</i> -21			H	780	NA	NA
22			H	2,200	> 10,000	NA
23			H	3,900	> 10,000	NA
24			H	> 1,000	> 10,000	NA
25			H	1,100	> 10,000	NA
26			H	> 1,000	> 10,000	NA
27			H	> 1,000	> 10,000	NA
28 (LU13)			H	0.6	> 1,000	> 1,000
29			H	1.5	> 1,000	NA
30			H	3.9	> 1,000	NA

^a NA = Not Available

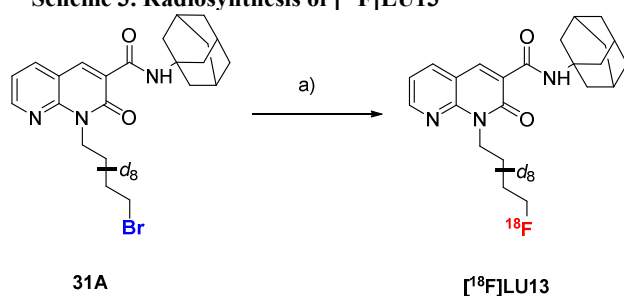
^b Reported in ref.⁴⁶

^c Reported in ref.⁴⁷

Radiochemistry. For the radiosynthesis of [¹⁸F]LU13, the bromo precursor **31** was synthesized in both deuterated (**31A**) and non-deuterated (**31B**) form. For biological evaluations, we decided to generate [¹⁸F]LU13 bearing a deuterated *N*-butyl chain for the introduction of fluorine-18 to reduce the risk of in vivo metabolic degradation which we observed for the structurally related analogue [¹⁸F]**5**. The non-deuterated precursor **31B** was used to establish the reaction conditions for radiofluorination. Compounds **31A** and **31B** were synthesized by the same synthetic route as described for LU13 (compound **28** in Scheme 2) by using 1,4-dibromobutane-*d*₈ or its non-deuterated analogue instead of 1-bromo-4-fluorobutane. The 1,4-dibromobutane-*d*₈ building block was obtained by dibrominative ring opening of tetrahydrofuran-*d*₈ according to the literature.⁵⁶ Before radiofluorination, precursor **31A**₆

was purified by HPLC. For an efficient production of [^{18}F]LU13, the reaction conditions were optimized by varying the amount of precursor **31B** (1 or 2 mg), the solvent (CH_3CN , DMF, DMSO), the radiofluorinating agent ($\text{K}[^{18}\text{F}]\text{F-K}_{2,2,2}$, [^{18}F]TBAF) and the temperature (range 90–150 °C). By using the Kryptofix-2.2.2 fluorinating complex $\text{K}[^{18}\text{F}]\text{F-K}_{2,2,2}$, only a trace amount of [^{18}F]LU13 were detected by radio-HPLC in any of the investigated solvents and temperatures. By using the milder radiofluorinating agent [^{18}F]TBAF, non-isolated [^{18}F]LU13 was detected in the range between 25% and 65% (radio-HPLC) in different solvents and temperatures. The most efficient formation of [^{18}F]LU13 was observed by using DMSO as solvent and a temperature of 120 °C. Based on these preliminary results, an automated radiosynthesis for [^{18}F]LU13 was developed on an Elysia-Raytest radiosynthesizer as depicted in Scheme 3. The purification of the product was performed by HPLC (Figure 3) followed by trapping the radiotracer [^{18}F]LU13 on a RP-cartridge and elution with EtOH. For biological experiments, the solvent was evaporated under a stream of nitrogen at 70 °C. The final product was formulated in sterile isotonic saline up to a final concentration of < 10% EtOH. The overall synthesis time was about 80 min. [^{18}F]LU13 was obtained with 25% radiochemical yield, high radiochemical purity (> 99%), and high molar activities in the range of 300–400 GBq/ μmol at the end of the synthesis ($n = 6$). No decomposition of the formulated product was observed within 24 h at room temperature. The identity of the final product [^{18}F]LU13 was confirmed with analytical HPLC by co-injection with the corresponding reference compound (Figure 3).

Scheme 3. Radiosynthesis of [^{18}F]LU13 ^a



^a Reagents and conditions: a) [^{18}F]TBAF, K_2CO_3 , DMSO, 120 °C, 10 min.

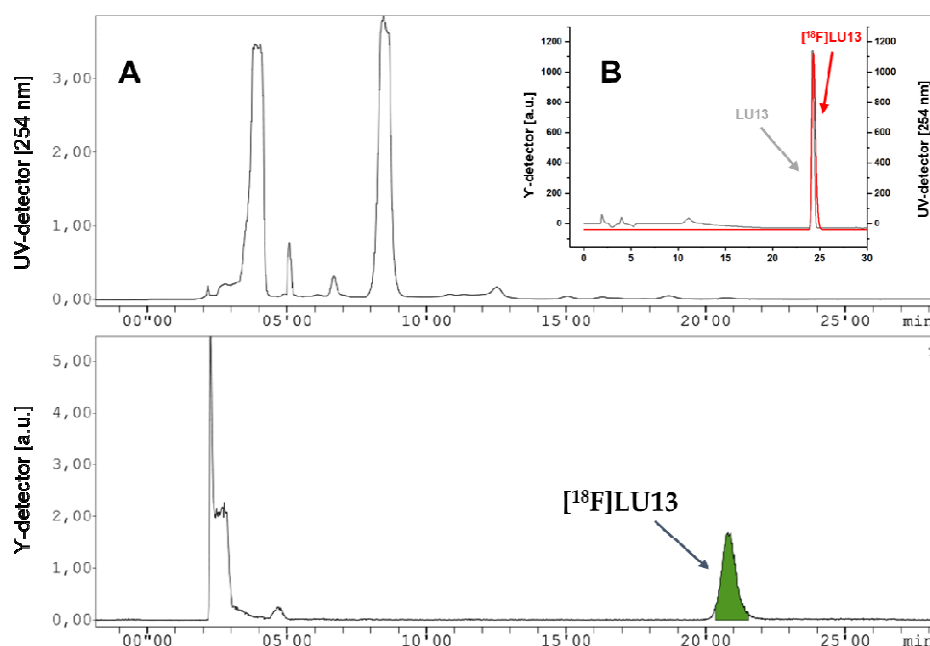


Figure 3. (A) Representative UV- and radio-HPLC chromatograms of [^{18}F]LU13 (conditions: Reprisil-Pur 120 C18-AQ (5 μm , 250x10 mm), 73% $\text{CH}_3\text{CN}/20 \text{ mM NH}_4\text{OAc}_{\text{aq}}$, 5 mL/min) and (B) Analytical radio- and UV-HPLC chromatogram of formulated [^{18}F]LU13 (conditions: Reprisil-Pur 120 C18-AQ (5 μm , 250x4.6 mm), 70% $\text{CH}_3\text{CN}/20 \text{ mM NH}_4\text{OAc}_{\text{aq}}$, 1 mL/min).

In Vitro Evaluation of [^{18}F]LU13. To verify the initially determined high affinity of LU13 by competitive radioligand binding assays and to investigate whether species effects might confound the following preclinical in vivo experiments, the equilibrium dissociation constants K_D of LU13 for human and rat CB2R were determined. Membrane preparations obtained from CHO cells stably transfected with human CB2R and from rat spleen were incubated with a single concentration of [^{18}F]LU13 along with non-radiolabeled LU13 at different concentrations. From the analyses of respective homologous competition curves (Fig. 4), reflecting the displacement of the radiolabeled ligand by the non-labeled ligand, K_D values of LU13 of 1.1 nM and 0.20 nM were estimated for human and rat CB2R (each as a single experiment run in triplicate), respectively, confirming a high affinity of [^{18}F]LU13 towards both human and rat. However, regardless of this encouraging finding, the receptor autoradiography performed in vitro with [^{18}F]LU13 and cryosections from rat spleen revealed only negligible specific binding of the radioligand towards CB2R (Fig. S1).⁷

Since we obtained a comparable result with the structurally related [^{18}F]5 previously,⁴⁶ we assume a fast dissociation of [^{18}F]LU13, and perhaps also of [^{18}F]5, from the rat CB2R as the main reason for the lack of specific binding in rat spleen *in vitro*.

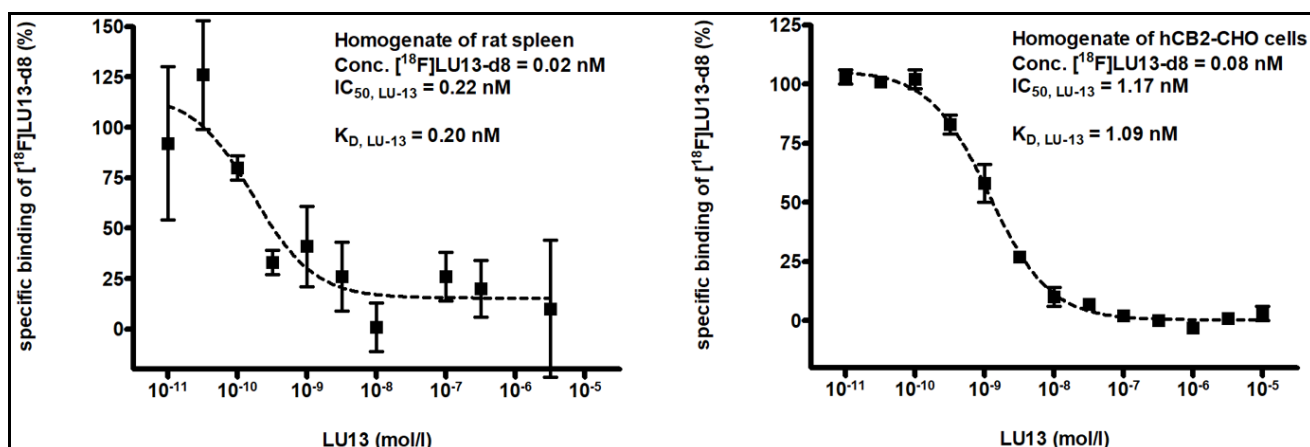


Figure 4. Determination of the equilibrium dissociation constants K_D of [^{18}F]LU13 for rat and human CB2R. The potential of LU13 to displace [^{18}F]LU13 from binding sites in homogenates of rat spleen (left) or CHO-cells stably transfected with human CB2R (right) has been investigated by homologous competition experiments. By nonlinear regression analysis of the respective competition curves, the respective IC_{50} values were estimated. The corresponding K_D values were calculated according to the simplified Cheng-Prusoff equation $K_D = K_I = \text{IC}_{50} - \text{concentration of the radioligand}$.⁵⁷

In Vivo Metabolism. The metabolism of [^{18}F]LU13 *in vivo* was investigated in female CD-1 mice by the radio-HPLC analyses of plasma, brain and spleen samples obtained at 30 min post-injection ($n = 3$). As shown in Figure 5, 23% of the activity in plasma corresponds to intact [^{18}F]LU13, while the remaining activity consists of only more polar radiometabolites. Confirming our working hypothesis to increase the metabolic stability by introducing a deuterated 4-fluorobutyl chain in [^{18}F]LU13^{51, 58}, a smaller fraction of radiometabolites has been detected for [^{18}F]LU13 compared with the structurally analogue [^{18}F]5⁴⁶ at this time-point (fraction of polar metabolites < 5% vs. 10%, respectively).

In the brain, $85 \pm 3\%$ of the activity corresponds to intact [^{18}F]LU13 (Figure 5 C). The remarkably high fraction of parent compound in the spleen ($94 \pm 5\%$) might be a hint of a CB2R-specific retention of the tracer in this organ. Overall, this preliminary evaluation revealed a high and, compared to the corresponding non-deuterated radioligand [^{18}F]5, improved metabolic stability of [^{18}F]LU13 *in vivo*.

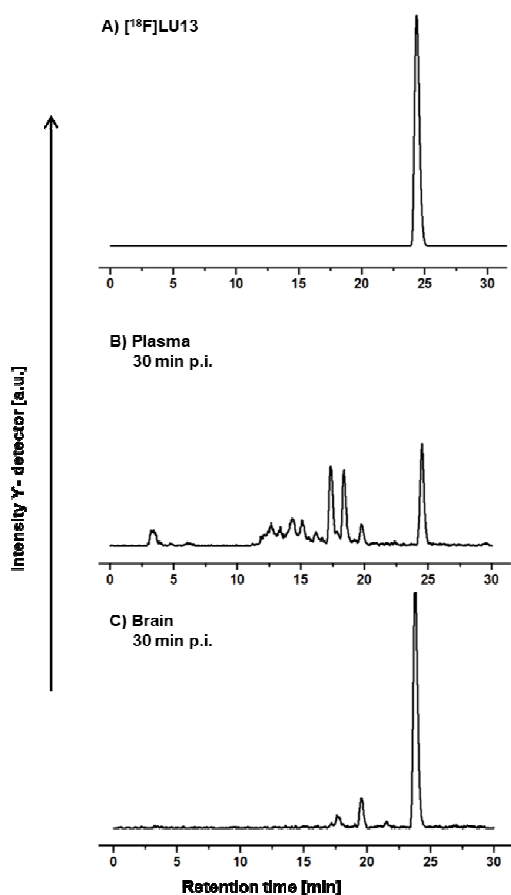


Figure 5. In vivo metabolism of [^{18}F]LU13. Analytical radio-HPLC chromatograms of tissue and organ samples of female CD-1 mice obtained at 30 min p.i.. (A) Representative HPLC chromatogram of [^{18}F]LU13; (B) Blood plasma samples [extraction with MeOH/H₂O (9:1); extraction yield: 95%]; (C) Brain homogenates [extraction with MeOH/H₂O (9:1); extraction yield: 96%]. HPLC conditions: Reprosil-Pur 120 C18-AQ (5 μm , 250x4.6 mm); gradient mode (10-90-10% CH₃CN/20 mM NH₄OAc_{aq}, 1 mL/min).

PET Imaging. The brain uptake, as well as the specific binding of [^{18}F]LU13 to the human CB2R was investigated in PET imaging experiments using a rat model with a local overexpression of hCB2R(D80N) in the right striatum, which has been already previously applied for the characterization of CB2R-targeted radioligands by Vandeputte et al., Attili et al. and Teodoro et al.^{46, 52, 53} The analysis of the time-activity curves (TACs) revealed a significantly higher uptake of activity into the striatal region overexpressing the hCB2R reaching a stable SUV_{20-60min} of 3.6 ± 0.9 after 26 min p.i. in comparison to the contralateral region (TAC peak SUV = 1.7 ± 0.3 , $p = 0.014$) and the cerebellum (TAC peak SUV = 1.8 ± 0.3 , $p = 0.016$) after i.v. injection of [^{18}F]LU13. We determined a mean time-to-peak of 6.1 min and 5.4 min ($p < 0.001$ vs. time-to-plateau frame SUV_{20-60min} in the target region) and a mean residence time (MRT) of 23 min of the radiotracer in the reference regions. (Figure 6 and Table 2). Based on these initial findings, we conclude that [^{18}F]LU13 crosses the BBB and most likely binds specifically to the hCB2R. In comparison to [^{18}F]5, another CB2R-targeted radioligand recently reported by us,⁴⁶ the high and stable concentration of activity in the target region between 20 and 60 minutes p.i. makes [^{18}F]LU13 more suitable for static PET imaging.

The signal-to-background ratio (SUVr) increased almost linearly during the period of investigation with a slope of 0.12 SUV/min ($r^2 = 0.94$) for the target region normalized to control, and a slope of 0.15 SUV/min ($r^2 = 0.80$) for the target region normalized to the cerebellum. Hence, a static PET imaging at later timepoints would be more preferable, whereby at 60 min p.i. a SUVr of 7.8 ± 1.6 for the target region-to-control and of 8.8 ± 4.3 for the target region-to-cerebellum were obtained, which are slightly higher compared to [^{18}F]5⁴⁶. In both reference regions the activity concentration over time (area under the curve, AUC) of [^{18}F]LU13 was 3.8 times lower compared to the target region (Table 2) and confirmed the use of the contralateral region and cerebellum as eligible reference regions in the animal model, as already shown by the use of [^{18}F]5⁴⁶ (Table 2).

To further prove the target specificity as well as the reversibility of [^{18}F]LU13 binding, we performed displacement experiments. Intravenous administration of GW405833, a potent and selective CB2R partial agonist, at 20 min after application of the radioligand resulted in washout of activity from the target region while the kinetics of [^{18}F]LU13 in the reference regions remained in general unaffected (Figure 6B, lower left graph). However, a slight increase of the radioactivity signal in the reference regions could be observed directly after the injection of blocking compound (AUC_{20-40min} of 21 vs. 28, $p = 0.122$; and of 18 vs. 28, $p = 0.013$; vehicle vs. GW405833, respectively; Figure 6A and S2). This could be explained by the redistribution of the brain hCB2R-D80N overexpressing region and peripheral bound [^{18}F]LU13 set free by the displacement with the blocking compound, as stated already previously for other CB2R radioligands.⁵³ The normalized AUC_{20-60min} were reduced (Fig. 6B, lower right) by 56.2% for the target re-9

gion-to-contralateral and 63.5% for the target region-to-cerebellum in comparison to the vehicle-treated animals (Table 3).

In summary, these results demonstrate a specific and reversible binding of [^{18}F]LU13 towards the hCB2R with a more favorable kinetics compared to our previously published CB2R-directed radioligand [^{18}F]5. Moreover, the strong accumulation in the brain region of CB2R overexpression proves its superior ability to image the cerebral CB2R when compared to the radioligands previously evaluated in this animal model.^{52, 53} Thus we conclude, that the radioligand [^{18}F]LU13 has a high potential for the non-invasive assessment of disease-related overexpression of CB2R in the brain by PET.

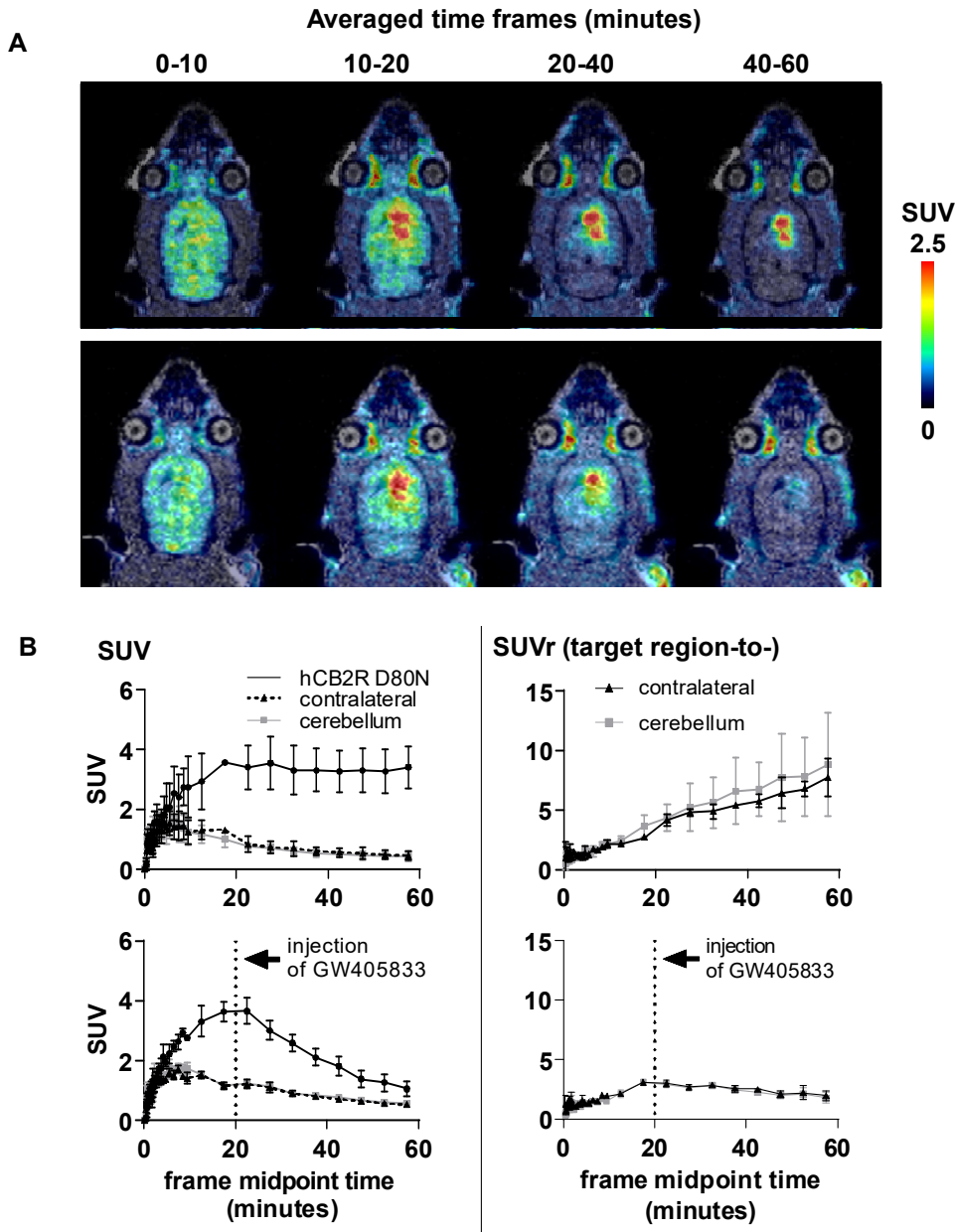


Figure 6. PET imaging of [^{18}F]LU13 in a rat model of local hCB2R overexpression in the right striatal region of the brain. (A) Representative coronal planes showing merged MR and PET images of averaged time frames of the control group (upper row) and displacement study (lower row), (B) TACs of the right (target region, hCB2R D80N) and the reference regions left striatum (contralateral), as well as of the cerebellum on the left side and the SUV hCB2R D80N normalized to control or cerebellum (SUVr) on the right side, of the vehicle-treated group (upper row, n = 3) and of the displacement studies (lower row) with GW405833 (5mg/kg, n = 3) injected (i.v.) at 20 min. p.i. of [^{18}F]LU13.

Table 2. Non-compartmental analysis of TACs, obtained from the regions of local overexpression of the hCB2R(D80N) in the right striatum of rats, the contralateral region in the left striatum, and the cerebellum after i.v. injection of [¹⁸F]LU13 (n = 3).

TAC parameter	hCB2R(D80N)	Contralateral	p-Value vs. hCB2R(D80N)	Cerebellum	p-Value vs. hCB2R(D80N)
Time-to-peak (min)	26 ± 3	6.1 ± 2.2	0.027	5.4 ± 2.8	0.026
TAC peak value (SUV)	3.6 ± 0.8	1.7 ± 0.3	0.011	1.8 ± 0.3	0.013
AUC (SUV · min)	178 ± 39	49 ± 12	0.003	46 ± 6	0.002
MRT (min)		23 ± 1		23 ± 3	

Mean ± SD; p-value - one-sided Student's *t*-test; TAC – Time activity curve, AUC -Area under the curve, MRT – Mean residence time

Table 3. Uptake of [¹⁸F]LU13 into the hCB2R overexpressing right striatum normalized to the contralateral left striatum as well as cerebellum (SUV ratio, SUVr) with (n = 3) or without (vehicle, n = 3) administration of GW405833 (5mg/kg bodyweight, i.v.) at 20 minutes after radiotracer administration, expressed as area under the curve before (AUC_{0-20min}) and after (AUC_{20-60min}) injection of the interventional drug.

hCB2R D80N-to-	Treatment	AUC _{0-20min} (CI _{95%}) in SUVr · min	AUC _{20-60min} (CI _{95%}) in SUVr · min
Contralateral	Vehicle	33 (31–34)	201 (187–215)
	Displacement	33 (31–34)	88 (82–94); - 56.2 %
Cerebellum	Vehicle	35 (30–40)	233 (181–284)
	Displacement	31 (29–33)	85 (80–91); - 63.5 %

Mean; 95% confidence interval (CI_{95%}).

CONCLUSIONS

Aiming at the development of a novel CB2R-targeting PET tracer with improved binding properties, we developed a novel series of fluorinated derivatives starting from the structure of our previously published radioligand [¹⁸F]5. By a systematic structure-affinity study we identified LU13, binding to CB2R with the highest affinity of 0.6 nM and possessing sufficient selectivity vs. CB1R (selectivity index > 1,000), as the most promising candidate. [¹⁸F]LU13 was obtained by radiolabeling of the corresponding bromo precursor 31 with [¹⁸F]TBAF. First biological evaluation of [¹⁸F]LU13 revealed excellent and species-independent affinity towards both hCB2R and rCB2R in vitro. In vivo, [¹⁸F]LU13 possesses a high metabolic stability in mice with only trace amounts of radiometabolites detectable in brain and spleen at 30 min post-injection. PET experiments in a rat model of a local human CB2R overexpression in the brain revealed that [¹⁸F]LU13 is able to cross the blood-brain barrier (BBB) and binds to hCB2R in a reversible manner. Considering the high CB2R affinity and selectivity, the high metabolic stability and the favorable kinetics in the brain, [¹⁸F]LU13 represents a very promising radiotracer for the detection of CB2R upregulation in neurological disorders.

EXPERIMENTAL SECTION

General Information

All chemicals and reagents were purchased from commercially available sources and used without further purification. Moisture-sensitive reactions were conducted under argon with oven-dried glassware and anhydrous solvents. Reaction progress was monitored by thin-layer chromatography (TLC) using Alugram® SIL G/UV₂₅₄ pre-coated plates (Macherey-Nagel; Düren; Germany). The spots were identified by using a UV lamp or by dipping the plates into a potassium permanganate solution (3 g KMnO₄, 20 g K₂CO₃, 0.25 mL glacial acid, 300 mL water). For purification of products flash column chromatography was used with silica gel 40 – 63 μm (VWR International Chemicals, Darmstadt; Germany). ¹H-, ¹³C- and ¹⁹F-NMR spectra were recorded on VARIAN Mercury plus (300 MHz for ¹H-NMR, 75 MHz for ¹³C-NMR, 282 MHz for ¹⁹F-NMR) and BRUKER DRX-400 (400 MHz for ¹H-NMR, 100 MHz for ¹³C-NMR, 377 MHz for ¹⁹F-NMR); chemical shifts (δ) in parts per million (ppm) are related to internal tetramethylsilane and coupling constants (*J*) are given with 0.1 Hz. High resolution mass spectra (HRFT-MS) were recorded on a FT-ICR APEX II spectrometer (Bruker Daltonics; Bruker Corporation; Billerica; USA) using electrospray ionization (ESI). The purity of all the tested compounds was ≥95% as determined by HPLC [Jasco, MD-2010Plus, LG-2080-04S, DG-2080-54, AS-2055Plus, LC-NetII/ADC, λ = 280 nm, column ReproSil-Pur Basic C18-HD (250 x 4.6 mm, 5 μm, Dr. Maisch GmbH), gradient MeCN/20mMAA from 10/90 to 90/10, to 10/90 (v/v) over 30 min, flowrate 1 mL/Min].

Chemical Synthesis

2-Amino-5-bromonicotinaldehyde (6) To a stirred solution of 2-aminopyridine-3-carboxaldehyde (17.6 g, 1 equiv, 144.4 mmol) in glacial acetic acid (685 mL) was added bromine (7 mL, 0.95 equiv, 137.2 mmol), and the reaction mixture was stirred at rt for 24 h. The precipitate obtained was filtered off and washed with ether. The filter cake was poured into water and treated with solid 11

NaOH until pH 7 – 8, and the mixture was extracted with dichloromethane. The organic layer was dried over anhydrous Na₂SO₄ and evaporated to dryness under reduced pressure to get a light yellow solid. The crude product was used without further purification. (**6**, 16.78 g, 83.5 mmol, 58%): ¹H NMR (DMSO-*d*₆): δ 9.83 (s, 1H, CHO), 8.30 (d, *J* = 2.5 Hz, 1H, Ar); 8.23 (d, *J* = 2.5 Hz, 1H, Ar); 7.69 (br, 2H, NH₂).

Ethyl-6-bromo-2-oxo-1,2-dihydro-1,8-naphthyridine-3-carboxylate (7) To a solution of **6** (16.8 g, 1 equiv, 83.5 mmol) in ethanol (220 mL) were added diethyl malonate (19.1 mL, 1.5 equiv, 125.2 mmol) and piperidine (2.4 mL, 2.1 g, 0.3 equiv, 24.2 mmol), and the mixture was stirred under reflux for 20 h. After cooling, the solid obtained was filtered, washed with ethanol, and dried under rotary vacuum. The crude product was used without further purifications (**6**, 20.5 g, 69.2 mmol, 83% yield): ¹H NMR (DMSO-*d*₆): δ 12.62 (br, 1H), 8.70 (d, *J* = 2.4 Hz, 1H), 8.56 (d, *J* = 2.5 Hz, 1H), 8.45 (s, 1H), 4.29 (q, *J* = 7.1 Hz, 2H), 1.30 (t, *J* = 7.1 Hz, 3H).

cis-/trans-6-Bromo-N-(4-methylcyclohexyl)-2-oxo-1,2-dihydro-1,8-naphthyridine-3-carboxamide (8) A mixture of **7** (6 g, 1 equiv, 20.18 mmol) and 4-methylcyclohexylamine (5.4 mL, 2 equiv, 40.4 mmol) was heated in a sealed tube at 150 °C for 24 h. After cooling, the reaction mixture was treated with diethyl ether to give a solid residue which was collected by filtration. The product was recrystallized from EA (**8**, 5.5 g, 15.2 mmol, 75% yield): ¹H NMR (DMSO-*d*₆): δ 12.09 (br, 1H), 10.06 and 9.57 (2m, 1H), 8.80 (m, 3H), 4.12 and 3.78 (2m, 1H), 1.90 (m, 12H).

General Procedure 1 for the N-Alkylation. A solution of appropriate starting material **8**, **9**, **17** or **19** (1 equiv) in anhydrous DMF (3 mL for 1 mmol of starting material) was treated with Cs₂CO₃ (3 equiv) at rt for 1 h. Then, the alkylating agent RX (2 equiv) was added and the reaction mixture was stirred for 12 h at 50 °C. After cooling, the reaction mixture was rotatory evaporated to give solid residue which was dissolved in EA and extracted with water (10 mL × 4). The combined organic layers were dried over anhydrous Na₂SO₄, filtered and concentrated by rotary evaporation. The obtained residue was purified by column chromatography (silica, EA:n-Hex).

cis-/trans-6-Bromo-1-(4-fluorobutyl)-N-(4-methylcyclohexyl)-2-oxo-1,2-dihydro-1,8-naphthyridine-3-carboxamide (15) General procedure 1, light yellow solid, 93.7% yield. ¹H NMR (300 MHz, CDCl₃) δ 9.92 and 9.54 (s, 1H), 8.79 (s, 1H), 8.70 (d, 1H), 8.17 (m, 1H), 4.61 (m, 2H), 4.43 (m, 2H), 4.23 and 3.87 (2m, 1H), 1.55 (m, 16H). ¹³C NMR (76 MHz, CDCl₃) δ 162.58, 161.73, 152.97, 148.55, 141.01, 140.07, 134.58, 130.02, 127.86, 124.73, 116.48, 114.52, 85.09, 82.90, 49.24, 46.06, 42.00, 34.22, 33.28, 32.33, 31.93, 31.40, 30.51, 29.92, 28.39, 28.15, 24.27, 23.00, 22.56, 21.86, 14.46. HRMS (ESI +) *m/z* for C₂₀H₂₅BrFN₃O₂⁺ 438.1241, calculated 438.1242.

cis-/trans-6-Bromo-1-(4-fluorobenzyl)-N-(4-methylcyclohexyl)-2-oxo-1,2-dihydro-1,8-naphthyridine-3-carboxamide (16) General procedure 1, beige solid, 98% yield. ¹H NMR (DMSO-*d*₆): δ 9.76 and 9.38 (d, 1H), 8.94 (m, 1H), 8.87 and 8.85 (m, 1H), 7.32 (m, 2H), 7.12 (m, 2H), 5.67 (s, 2H), 4.10 and 3.73 (2m, 1H), 1.62 (m, 14H). ¹³C NMR (101 MHz, CDCl₃) δ 163.68, 162.59, 161.48, 152.84, 148.44, 141.15, 140.99, 140.09, 130.84, 124.86, 116.47, 115.62, 115.41, 114.69, 49.21, 46.05, 44.47, 34.12, 33.15, 32.22, 31.20, 30.40, 29.76, 22.47, 21.73. HRMS (ESI +) *m/z* for C₂₃H₂₄BrFN₃O₂⁺ 472.1039, calculated 472.1039.

6-(Furan-2-yl)-N-(4-methylcyclohexyl)-2-oxo-1,2-dihydro-1,8-naphthyridine-3-carboxamide (9) To a solution of **8** (0.27 g, 0.70 mmol) in 3 ml of DMF were added tributyl(furan-2-yl)stannane (242 μl, 0.77 mmol) and Pd(Cl₂)(PPh₃)₂ (24.57 mg, 0.04 mmol) under Ar atmosphere. The mixture was stirred at 90 °C for 3h. The progress of the reaction was controlled by TLC (silica, EA/n-Hex/AcOH, 1:1:0.01). After cooling, the reaction mixture was quenched with 5% aqueous NaHCO₃ and filtered through celite. The filtrate was washed with CH₂Cl₂. The organic layer was separated and washed with brine, dried over Na₂SO₄, filtered and concentrated under reduced pressure. The product was purified by flash chromatography on silica gel (MeOH:CDCl₃, 1:50) and recrystallized from ethyl acetate (**9**, 100 mg, 0.3 mmol, 41% yield). ¹H NMR (400 MHz, DMSO-*d*₆) δ 12.99 (s, 2H), 10.00 (d, *J* = 7.9 Hz, 1H), 9.55 (d, *J* = 7.8 Hz, 1H), 9.04 (dd, *J* = 5.8, 2.3 Hz, 2H), 8.89 (d, *J* = 6.8 Hz, 2H), 8.66 (t, *J* = 2.3 Hz, 2H), 7.84 (d, *J* = 1.7 Hz, 2H), 7.10 (t, *J* = 3.5 Hz, 2H), 6.65 (m, 1H), 4.11 (s, 1H), 3.70 (m, 1H), 1.93 (m, 2H), 1.70 (m, 4H), 1.57 (m, 4H), 1.18 (m, 8H), 0.90 (dd, *J* = 12.7, 6.5 Hz, 6H).

trans-1-(4-Fluorobenzyl)-6-(furan-2-yl)-N-(4-methylcyclohexyl)-2-oxo-1,2-dihydro-1,8-naphthyridine-3-carboxamide (trans-10) General procedure 1, yellow solid 30% yield. ¹H NMR (400 MHz, CDCl₃) δ 9.55 (d, *J* = 8.1 Hz, 1H), 9.02 (d, *J* = 2.3 Hz, 1H), 8.92 (s, 1H), 8.28 (d, *J* = 2.4 Hz, 1H), 7.56 (dd, *J* = 1.8, 0.7 Hz, 1H), 7.45 (m, 2H), 7.96 (m, 2H), 6.79 (dd, *J* = 3.4, 0.7 Hz, 1H), 6.54 (dd, *J* = 3.4, 1.8 Hz, 1H), 5.78 (s, 2H), 3.92 (m, 1H), 2.07 (m, 3H), 1.76 (m, 2H), 1.32 (m, 3H), 1.11 (m, 2H), 0.92 (d, *J* = 6.5 Hz, 3H). ¹³C NMR (CDCl₃) δ 153.21, 152.51, 152.22, 148.51, 142.41, 141.55, 140.98, 138.68, 131.53, 130.36, 122.88, 121.98, 120.31, 112.44, 110.55, 108.21, 100.01, 50.41, 48.53, 32.49, 31.17, 30.98, 22.10. HRMS (ESI⁺): *m/z* = 460.2043, calcd. 460.2036 for C₂₇H₂₇FN₃O₃⁺ [M+H]⁺

cis-1-(4-Fluorobenzyl)-6-(furan-2-yl)-N-(4-methylcyclohexyl)-2-oxo-1,2-dihydro-1,8-naphthyridine-3-carboxamide (cis-10) General procedure 1, yellow solid, 33% yield. ¹H NMR (400 MHz, CDCl₃) δ 9.97 (d, *J* = 7.8 Hz, 1H), 9.04 (d, *J* = 2.3 Hz, 1H), 8.95 (s, 1H), 8.30 (d, *J* = 2.3 Hz, 1H), 7.58 (dd, *J* = 1.8, 0.7 Hz, 1H), 7.53 (m, 2H), 7.00 (m, 2H), 6.81 (dd, *J* = 3.4, 0.7 Hz, 1H), 6.57 (dd, *J* = 3.4, 1.8 Hz, 1H), 5.82 (s, 2H), 4.29 (m, 1H), 1.87 (m, 1H), 1.69 (m, 3H), 1.31 (m, 5H), 1.01 (d, *J* = 6.5 Hz, 3H). ¹³C NMR (CDCl₃) δ 162.11, 161.42, 160.21, 142.57, 140.47, 137.55, 135.88, 134.58, 131.43, 130.38, 127.57, 125.48, 120.31, 112.48, 110.45, 105.51, 100.21, 45.41, 44.53, 31.48, 30.17, 29.77, 21.15. HRMS (ESI⁺): *m/z* = 460.2041, calcd. 460.2036 for C₂₇H₂₇FN₃O₃⁺ [M+H]⁺

trans-1-(2-Fluorobenzyl)-6-(furan-2-yl)-N-(4-methylcyclohexyl)-2-oxo-1,2-dihydro-1,8-naphthyridine-3-carboxamide (trans-11) General procedure 1, yellow solid, 30%, yield ¹H NMR (400 MHz, CDCl₃) δ 9.51 (d, *J* = 8.1 Hz, 1H), 8.98 (s, 1H), 8.95 (d, *J* = 2.3 Hz, 1H), 8.31 (d, *J* = 2.3 Hz, 1H), 7.55 (d, *J* = 1.8 Hz, 1H), 7.20 (m, 1H), 7.09 (m, 1H), 6.97 (m, 1H), 6.85 (m, 1H), 6.77 (d, *J* = 3.4 Hz, 1H), 6.53 (dd, *J* = 3.4, 1.8 Hz, 1H), 5.89 (s, 2H), 3.92 (m, 1H), 2.06 (m, 2H), 1.75 (m, 2H), 1.32 (m, 3H), 1.09 (m, 2H), 0.90 (m, 3H). ¹³C NMR (CDCl₃) δ 161.21, 160.45, 153.21, 151.53, 145.47, 140.25, 139.88, 135.48, 131.23, 130.38, 125.57, 122.47, 121.31, 120.78, 112.45, 110.41, 108.21, 105.41, 101.22, 48.53, 40.68, 34.17, 33.77, 32.17, 21.25. HRMS (ESI⁺): *m/z* = 460.2033, calcd. 460.2036 for C₂₇H₂₇FN₃O₃⁺ [M+H]⁺

cis-1-(2-Fluorobenzyl)-6-(furan-2-yl)-N-(4-methylcyclohexyl)-2-oxo-1,2-dihydro-1,8-naphthyridine-3-carboxamide (cis-11) General procedure 1, yellow solid, 26% yield. ¹H NMR (400 MHz, CDCl₃) δ 9.88 (d, *J* = 7.8 Hz, 1H), 8.98 (s, 1H), 8.94 (d, *J* = 2.3 Hz, 1H), 8.30 (d, *J* = 2.3 Hz, 1H), 7.55 (d, *J* = 1.8 Hz, 1H), 7.21 (m, 1H), 7.09 (m, 1H), 6.97 (m, 1H), 6.86 (m, 1H), 6.76 (d, *J* = 3.4 Hz,

1H), 6.53 (dd, $J = 3.4, 1.8$ Hz, 1H), 5.91 (s, 2H), 4.26 (m, 1H), 1.82 (m, 2H), 1.68 (m, 3H), 1.28 (m, 4H), 0.95 (d, $J = 6.4$ Hz, 3H). ^{13}C NMR (CDCl_3) δ 150.22, 149.67, 148.31, 141.43, 140.87, 139.25, 136.88, 135.78, 130.23, 128.47, 125.58, 123.47, 122.51, 118.76, 115.14, 110.72, 109.27, 108.43, 100.21, 42.13, 40.77, 31.17, 30.50, 30.11, 21.23. HRMS (ESI^+): $m/z = 460.2036$, calcd. 460.2036 for $\text{C}_{27}\text{H}_{27}\text{FN}_3\text{O}_3^+$ [$\text{M}+\text{H}$] $^+$

trans-1-(2-Fluorobenzyl)-6-(furan-2-yl)-*N*-(4-methylcyclohexyl)-2-oxo-1,2-dihydro-1,8-naphthyridine-3-carboxamide (*trans*-12) General procedure 1, yellow solid, 30% yield. ^1H NMR (400 MHz, CDCl_3) δ 9.51 (d, $J = 8.1$ Hz, 1H), 8.98 (s, 1H), 8.95 (d, $J = 2.3$ Hz, 1H), 8.31 (d, $J = 2.3$ Hz, 1H), 7.55 (d, $J = 1.8$ Hz, 1H), 7.20 (m, 1H), 7.09 (m, 1H), 6.97 (m, 1H), 6.85 (m, 1H), 6.77 (d, $J = 3.4$ Hz, 1H), 6.53 (dd, $J = 3.4, 1.8$ Hz, 1H), 5.89 (s, 2H), 3.92 (m, 1H), 2.06 (m, 2H), 1.75 (m, 2H), 1.30 (m, 3H), 1.09 (m, 2H), 0.90 (m, 3H). ^{13}C NMR (CDCl_3) δ 161.21, 160.45, 153.21, 151.53, 145.47, 140.25, 139.88, 135.48, 131.23, 130.38, 125.57, 122.47, 121.31, 120.78, 112.45, 110.41, 108.21, 105.41, 101.22, 48.53, 40.68, 34.17, 33.77, 32.17, 21.25. HRMS (ESI^+): $m/z = 460.2033$, calcd. 460.2036 for $\text{C}_{27}\text{H}_{27}\text{FN}_3\text{O}_3^+$ [$\text{M}+\text{H}$] $^+$

cis-1-(2-Fluorobenzyl)-6-(furan-2-yl)-*N*-(4-methylcyclohexyl)-2-oxo-1,2-dihydro-1,8-naphthyridine-3-carboxamide (*cis*-12) General procedure 1, yellow solid, 26% yield. ^1H NMR (400 MHz, CDCl_3) δ 9.88 (d, $J = 7.8$ Hz, 1H), 8.98 (s, 1H), 8.94 (d, $J = 2.3$ Hz, 1H), 8.30 (d, $J = 2.3$ Hz, 1H), 7.55 (d, $J = 1.8$ Hz, 1H), 7.21 (m, 1H), 7.09 (m, 1H), 6.97 (m, 1H), 6.86 (m, 1H), 6.76 (d, $J = 3.4$ Hz, 1H), 6.53 (dd, $J = 3.4, 1.8$ Hz, 1H), 5.91 (s, 2H), 4.26 (m, 1H), 1.83 (m, 2H), 1.67 (m, 3H), 1.28 (m, 4H), 0.95 (d, $J = 6.4$ Hz, 3H). ^{13}C NMR (CDCl_3) δ 150.22, 149.67, 148.31, 141.43, 140.87, 139.25, 136.88, 135.78, 130.23, 128.47, 125.58, 123.47, 122.51, 118.76, 115.14, 110.72, 109.27, 108.43, 100.21, 42.13, 40.77, 31.17, 30.50, 30.11, 21.23. HRMS (ESI^+): $m/z = 460.2036$, calcd. 460.2036 for $\text{C}_{27}\text{H}_{27}\text{FN}_3\text{O}_3^+$ [$\text{M}+\text{H}$] $^+$

trans-1-(3-Fluoropropyl)-6-(furan-2-yl)-*N*-(4-methylcyclohexyl)-2-oxo-1,2-dihydro-1,8-naphthyridine-3-carboxamide (*trans*-13) General procedure 1, yellow solid, 24% yield. ^1H NMR (400 MHz, CDCl_3) δ 9.59 (d, $J = 8.0$ Hz, 1H), 9.01 (d, $J = 2.3$ Hz, 1H), 8.91 (s, 1H), 8.28 (d, $J = 2.3$ Hz, 1H), 7.56 (dd, $J = 1.9, 0.7$ Hz, 1H), 6.79 (dd, $J = 3.4, 0.8$ Hz, 1H), 6.55 (dd, $J = 3.4, 1.8$ Hz, 1H), 4.78 (m, 2H), 4.67 (t, $J = 5.8$ Hz, 1H), 4.55 (t, $J = 5.8$ Hz, 1H), 3.93 (m, 1H), 2.21 (m, 2H), 1.76 (m, 2H), 1.37 (m, 4H), 1.11 (m, 3H), 0.92 (d, $J = 6.5$ Hz, 3H). ^{13}C NMR (CDCl_3) δ 160.31, 159.21, 140.52, 135.48, 134.25, 131.77, 130.82, 121.28, 120.38, 111.87, 110.92, 108.31, 101.21, 86.57, 85.22, 50.27, 40.21, 33.41, 32.49, 31.53, 30.18, 21.55. HRMS (ESI^+): $m/z = 412.2043$, calcd. 412.2036 for $\text{C}_{23}\text{H}_{27}\text{FN}_3\text{O}_3^+$ [$\text{M}+\text{H}$] $^+$

cis-1-(3-Fluoropropyl)-6-(furan-2-yl)-*N*-(4-methylcyclohexyl)-2-oxo-1,2-dihydro-1,8-naphthyridine-3-carboxamide (*cis*-13) General procedure 1, yellow solid, 35% yield. ^1H NMR (400 MHz, CDCl_3) δ 9.96 (d, $J = 7.9$ Hz, 1H), 9.01 (d, $J = 2.3$ Hz, 1H), 8.91 (s, 1H), 8.27 (d, $J = 2.3$ Hz, 1H), 7.56 (dd, $J = 1.8, 0.7$ Hz, 1H), 6.79 (dd, $J = 3.4, 0.7$ Hz, 1H), 6.55 (dd, $J = 3.4, 1.8$ Hz, 1H), 4.78 (dd, $J = 8.4, 6.2$ Hz, 2H), 4.68 (t, $J = 5.9$ Hz, 1H), 4.56 (t, $J = 5.9$ Hz, 1H), 4.26 (m, 1H), 2.23 (m, 2H), 1.84 (m, 2H), 1.66 (m, 4H), 1.30 (m, 3H), 0.98 (d, $J = 6.5$ Hz, 3H). ^{13}C NMR (CDCl_3) δ 162.41, 150.22, 149.51, 149.41, 142.55, 131.98, 122.68, 114.53, 106.36, 83.88, 80.98, 60.31, 39.44, 34.55, 30.21, 30.01, 29.41, 27.53, 27.49, 22.17, 19.98. HRMS (ESI^+): $m/z = 412.2043$, calcd. 412.2036 for $\text{C}_{23}\text{H}_{26}\text{FN}_3\text{O}_3^+$ [$\text{M}+\text{H}$] $^+$

trans-1-(4-Fluorobutyl)-6-(furan-2-yl)-*N*-(4-methylcyclohexyl)-2-oxo-1,2-dihydro-1,8-naphthyridine-3-carboxamide (*trans*-14) General procedure 1, yellow solid, 70% yield. ^1H NMR (400 MHz, CDCl_3) δ 9.62 (d, $J = 8.1$ Hz, 1H), 9.01 (d, $J = 2.3$ Hz, 1H), 8.90 (s, 1H), 8.27 (d, $J = 2.3$ Hz, 1H), 7.56 (dd, $J = 1.8, 0.7$ Hz, 1H), 6.79 (dd, $J = 3.4, 0.8$ Hz, 1H), 6.55 (dd, $J = 3.4, 1.8$ Hz, 1H), 4.64 (t, $J = 7.3$ Hz, 2H), 4.61 – 4.56 (t, $J = 5.6$ Hz, 1H), 4.47 (t, $J = 5.9$ Hz, 1H), 3.92 (m, 3.9 Hz, 1H), 2.07 (m, 2H), 1.85 (m, 5H), 1.32 (m, 4H), 1.11 (m, 2H), 0.92 (d, $J = 6.5$ Hz, 3H). ^{13}C NMR (CDCl_3) δ 162.51, 153.22, 150.11, 148.51, 147.55, 141.63, 131.88, 123.68, 122.96, 114.63, 106.36, 78.88, 49.31, 41.12, 34.55, 33.21, 32.01, 29.41, 27.53, 27.49, 24.51, 22.17. HRMS (ESI^+): $m/z = 426.2224$, calcd. 426.2193 for $\text{C}_{24}\text{H}_{29}\text{FN}_3\text{O}_3^+$ [$\text{M}+\text{H}$] $^+$

cis-1-(4-Fluorobutyl)-6-(furan-2-yl)-*N*-(4-methylcyclohexyl)-2-oxo-1,2-dihydro-1,8-naphthyridine-3-carboxamide (*cis*-14) Yellow solid, 96% yield. ^1H NMR (400 MHz, CDCl_3) δ 9.99 (d, $J = 7.7$ Hz, 1H), 9.01 (d, $J = 2.3$ Hz, 1H), 8.91 (s, 1H), 8.27 (d, $J = 2.3$ Hz, 1H), 7.56 (d, $J = 1.7$ Hz, 1H), 6.79 (dd, $J = 3.4, 0.8$ Hz, 1H), 6.55 (dd, $J = 3.5, 1.8$ Hz, 1H), 4.66 (t, $J = 7.3$ Hz, 2H), 4.60 (t, $J = 5.6$ Hz, 1H), 4.48 (t, $J = 5.9$ Hz, 1H), 4.27 (m, 1H), 1.88 (m, 5H), 1.66 (m, 3H), 1.30 (m, 5H), 0.99 (d, $J = 6.5$ Hz, 3H). ^{13}C NMR (101 MHz, CDCl_3) δ 161.78, 150.01, 148.46, 147.98, 143.22, 141.63, 132.22, 123.77, 122.95, 114.60, 111.98, 106.36, 82.89, 45.67, 41.44, 31.03, 30.18, 29.58, 28.04, 27.84, 23.97, 23.91, 21.47. HRMS (ESI^+): $m/z = 426.2205$, calcd. 426.2193 for $\text{C}_{24}\text{H}_{29}\text{FN}_3\text{O}_3^+$ [$\text{M}+\text{H}$] $^+$

Ethyl-2-oxo-1,2-dihydro-1,8-naphthyridine-3-carboxylate (**17**) Diethylmalonate (9.4 mL, 9.9 g, 61.6 mmol, 2.5 equiv) and piperidine (6 mL, 5.2 g, 60.6 mmol, 2.5 equiv) were added to a solution of 2-aminopyridine-3-carbaldehyde (3 g, 24.6 mmol, 1 equiv) in 60 mL EtOH. The reaction mixture was stirred for 19 h under reflux. The yellow suspension was filtered at RT, washed with EtOH and concentrated under reduced pressure giving the light-yellow solid **17** in 81% yield (4.34 g, 19.9 mmol). ^1H NMR (400 MHz, $\text{DMSO}-d_6$) δ = 1.30 (t, $J = 7.1$ Hz, 3H), 4.28 (q, $J = 7.1$ Hz, 2H), 7.29 (dd, $J = 7.8, 4.7$ Hz, 1H), 8.27 (dd, $J = 7.9, 1.8$ Hz, 1H), 8.49 (s, 1H), 8.60 (dd, $J = 4.7, 1.8$ Hz, 1H), 12.43 (s, 1H).

Ethyl-1-(4-fluorobutyl)-2-oxo-1,2-dihydro-1,8-naphthyridine-3-carboxylate (**18**) 1-Bromo-4-fluorobutane (0.980 mL, 1.42 g, 9.13 mmol, 2.00 equiv) was added to a mixture of ethyl-2-oxo-1,2-dihydro-1,8-naphthyridine-3-carboxylate (**17**, 0.998 g, 4.57 mmol, 1.00 equiv) and anhydrous K_2CO_3 (3.17 g, 22.9 mmol, 5.01 equiv) in 100 mL DMF. The reaction mixture was stirred for 19 h at 90°C and extracted with NaHCO_3 (5%) and CH_2Cl_2 . The organic layer was dried over MgSO_4 and filtered. Afterwards, the solvent was evaporated under reduced pressure and the obtained solid was recrystallized with Et_2O . The product was obtained in 87% yield (1.17 g, 3.99 mmol) as a light-brown solid. ^1H NMR (400 MHz, CDCl_3) δ = 1.41 (t, $J = 7.1$ Hz, 3H), 1.85 (m, 4H), 4.43 (q, $J = 7.1$ Hz, 2H), 4.44 (t, $J = 5.9$ Hz, 1H), 4.55 (t, $J = 5.6$ Hz, 1H), 4.59 (t, $J = 7.3$ Hz, 2H), 7.21 (dd, $J = 7.7, 4.7$ Hz, 1H), 7.96 (dd, $J = 7.7, 1.9$ Hz, 1H), 8.33 (s, 1H), 8.68 (dd, $J = 4.7, 1.9$ Hz, 1H).

1-(4-Fluorobutyl)-2-oxo-1,2-dihydro-1,8-naphthyridine-3-carboxylic acid (**32**) Ethyl-1-(4-fluorobutyl)-2-oxo-1,2-dihydro-1,8-naphthyridine-3-carboxylate (**18**, 0.980 g, 3.35 mmol, 1.00 equiv) and $\text{LiOH}\cdot\text{H}_2\text{O}$ (0.422 g, 10.1 mmol, 3.00 equiv) were dissolved in 20 mL of a mixture of THF:MeOH:H₂O (2:1:1, v/v/v) and stirred for 2 h at 60°C. Half of the solvent was removed under reduced pressure. 5 mL of water and hydrochloric acid (3M) were added until a pH of 1 was reached. After filtration and washing of the

precipitation with hydrochloric acid (1M), the white solid was dried to yield 88% (0.777 g, 2.94 mmol) of compound **32**. ¹H NMR (300 MHz, CDCl₃): δ = 1.89 (m, 4H), 4.45 (t, *J* = 5.8 Hz, 1H), 4.60 (t, *J* = 5.7 Hz, 1H), 4.70 (m, 2H), 7.41 (dd, *J* = 7.8, 4.6 Hz, 1H), 8.16 (dd, *J* = 7.9, 1.8 Hz, 1H), 8.82 (dd, *J* = 4.7, 1.9 Hz, 1H), 8.91 (s, 1H), 14.34 (s, 1H).

General procedure 2 for the synthesis of carboxamides 22-28 1-(4-Fluorobutyl)-2-oxo-1,2-dihydro-1,8-naphthyridine-3-carboxylic acid (**32**, 0.110-0.242 mmol, 1.00 equiv) and BOP (1.1-1.5 equiv) were dissolved with 1-10 mL CH₂Cl₂ and stirred at rt. Triethylamine (3 equiv) and the appropriate amine (1.00 equiv) were added. The reaction mixture was stirred for 16 h at RT. The reaction mixture was extracted with H₂O, NaHCO₃ and EA. Subsequently, the organic layer was washed with brine and dried over MgSO₄. After filtration and concentration through evaporation the obtained residue was purified by column chromatography (silica, EA:*n*-Hex). Solvent removal under reduced pressure yielded the corresponding target compounds.

trans-1-(3-Fluoropropyl)-N-(4-methylcyclohexyl)-2-oxo-1,2-dihydro-1,8-naphthyridine-3-carboxamide (trans-20) General procedure 1, white solid, 30% yield. ¹H NMR (400 MHz, CDCl₃) δ 9.59 (d, *J* = 8.0 Hz, 1H), 8.87 (s, 1H), 8.71 (dd, *J* = 4.7, 1.9 Hz, 1H), 8.08 (dd, *J* = 7.8, 1.9 Hz, 1H), 7.28 (dd, *J* = 7.8, 4.7 Hz, 1H), 4.76 (m, 2H), 4.66 (t, *J* = 5.9 Hz, 1H), 4.54 (t, *J* = 5.9 Hz, 1H), 3.92 (m, 1H), 2.20 (m, 2H), 2.06 (m, 2H), 1.76 (m, 2H), 1.33 (m, 3H), 1.10 (m, 2H), 0.92 (d, *J* = 6.5 Hz, 3H). ¹³C NMR (101 MHz, CDCl₃) δ 162.61, 161.82, 152.04, 149.69, 142.00, 138.47, 123.22, 119.14, 114.99, 83.01, 81.36, 48.82, 33.92, 32.98, 32.01, 28.97, 22.25. HRMS (ESI⁺): *m/z* = 346.1936, calcd. 346.1931 for C₁₉H₂₅FN₃O₂⁺ [M+H]⁺

cis-1-(3-Fluoropropyl)-N-(4-methylcyclohexyl)-2-oxo-1,2-dihydro-1,8-naphthyridine-3-carboxamide (cis-20) General procedure 1, white solid, 33% yield. ¹H NMR (400 MHz, CDCl₃) δ 9.96 (d, *J* = 7.8 Hz, 1H), 8.88 (s, 1H), 8.71 (dd, *J* = 4.7, 1.9 Hz, 1H), 8.08 (dd, *J* = 7.7, 1.9 Hz, 1H), 7.28 (dd, *J* = 7.8, 4.7 Hz, 1H), 4.77 (m, 2H), 4.67 (t, *J* = 5.9 Hz, 1H), 4.56 (t, *J* = 6.0 Hz, 1H), 4.26 (m, 1H), 2.22 (m, 2H), 1.85 (m, 2H), 1.66 (m, 4H), 1.30 (m, 3H), 0.98 (d, *J* = 6.6 Hz, 3H). ¹³C NMR (101 MHz, CDCl₃) δ 162.66, 161.82, 152.00, 149.74, 141.83, 138.43, 123.30, 119.09, 114.97, 83.09, 81.45, 45.69, 31.04, 30.20, 29.60, 28.96, 21.48. HRMS (ESI⁺): *m/z* = 346.1926, calcd. 346.1931 for C₁₉H₂₅FN₃O₂⁺ [M+H]⁺

trans-1-(2-(2-Fluoroethoxy)ethyl)-N-(4-methylcyclohexyl)-2-oxo-1,2-dihydro-1,8-naphthyridine-3-carboxamide (trans-21) General procedure 1, white solid, 35% yield. ¹H NMR (400 MHz, DMSO-*d*₆) δ 9.51 (d, *J* = 7.8 Hz, 1H), 8.88 (s, 1H), 8.78 (dd, *J* = 4.7, 1.8 Hz, 1H), 8.49 (dd, *J* = 7.8, 1.9 Hz, 1H), 7.45 (dd, *J* = 7.8, 4.7 Hz, 1H), 4.70 (t, *J* = 6.7 Hz, 2H), 4.54 (m, 1H), 4.40 (m, 1H), 3.77 (m, 4H), 3.63 (m, 1H), 1.93 (d, *J* = 11.8 Hz, 2H), 1.70 (d, *J* = 12.9 Hz, 2H), 1.31 (m, 3H), 1.07 (m, 2H), 0.89 (d, *J* = 6.5 Hz, 3H). ¹³C NMR (101 MHz, DMSO-*d*₆) δ 162.44, 161.55, 152.78, 149.67, 142.58, 139.89, 122.78, 119.93, 115.02, 84.23, 82.58, 70.06, 67.22, 48.50, 32.81, 31.81, 31.14, 22.54. HRMS (ESI⁺): *m/z* = 376.2035, calcd. 376.2036 for C₂₀H₂₇FN₃O₃⁺ [M+H]⁺

cis-1-(2-(2-Fluoroethoxy)ethyl)-N-(4-methylcyclohexyl)-2-oxo-1,2-dihydro-1,8-naphthyridine-3-carboxamide (cis-21) General procedure 1, white solid (41%). ¹H NMR (400 MHz, DMSO-*d*₆) δ 9.89 (d, *J* = 7.7 Hz, 1H), 8.90 (d, *J* = 8.7 Hz, 1H), 8.79 (dt, *J* = 5.2, 2.6 Hz, 1H), 8.50 (dd, *J* = 7.8, 1.9 Hz, 1H), 7.46 (dd, *J* = 7.7, 4.7 Hz, 1H), 4.72 (dt, *J* = 12.3, 6.6 Hz, 2H), 4.54 (m, 1H), 4.41 (m, 1H), 4.10 (m, 1H), 3.75 (t, *J* = 6.2 Hz, 3H), 3.67 (t, *J* = 4.0 Hz, 1H), 1.75 (m, 2H), 1.50 (m, 4H), 1.24 (m, 3H), 0.93 (d, *J* = 7.38 Hz, 3H). ¹³C NMR (101 MHz, DMSO-*d*₆) δ 162.71, 161.48, 152.82, 149.69, 142.60, 139.92, 122.79, 119.98, 115.06, 84.26, 82.62, 70.04, 67.30, 45.00, 31.17, 30.16, 29.65, 22.11. HRMS (ESI⁺): *m/z* = 376.2048, calcd. 376.2036 for C₂₀H₂₇FN₃O₃⁺ [M+H]⁺

1-(4-Fluorobutyl)-2-oxo-N-phenyl-1,2-dihydro-1,8-naphthyridine-3-carboxamide (22) General procedure 2, white solid, 51% yield; ¹H NMR (400 MHz, CDCl₃): δ = 1.91 (m, 4H), 4.54 (dt, *J* = 47.6, 5.8 Hz, 2H), 4.70 (m, 2H), 7.15 (m, 1H), 7.32 (dd, *J* = 7.8, 4.7 Hz, 1H), 7.38 (m, 2H), 7.79 (m, 2H), 8.12 (dd, *J* = 7.8, 1.9 Hz, 1H), 8.75 (dd, *J* = 4.7, 1.9 Hz, 1H), 8.99 (s, 1H), 11.97 (s, 1H); ¹³C NMR (101 MHz, CDCl₃): δ = 24.1 (d, *J* = 5.3 Hz), 28.1 (d, *J* = 20.0 Hz), 41.7, 83.9 (d, *J* = 165.1 Hz), 115.1, 119.5, 120.8 (s, 2C), 123.2, 124.6 (s, 2C), 129.1 (s, 1/2C), 138.3, 138.8, 142.7, 149.9, 152.6, 160.9, 162.9; ¹⁹F NMR (282 MHz, CDCl₃): δ = -218.3 (1F); HRMS (ESI⁺) *m/z* for C₁₉H₁₈FN₃NaO₂⁺ [M + Na]⁺ 362.1295, calcd 362.1275.

1-(4-Fluorobutyl)-N-(4-fluorophenyl)-2-oxo-1,2-dihydro-1,8-naphthyridine-3-carboxamide (23) General procedure 2, light-yellow solid in 44% yield; ¹H NMR (300 MHz, CDCl₃): δ = 1.91 (m, 4H), 4.56 (dt, *J* = 47.2, 5.8 Hz, 2H), 4.70 (t, *J* = 7.5 Hz, 2H), 7.06 (m, 2H), 7.32 (dd, *J* = 7.8, 4.7 Hz, 1H), 7.75 (m, 2H), 8.12 (dd, *J* = 7.8, 1.9 Hz, 1H), 8.75 (dd, *J* = 4.7, 1.9 Hz, 1H), 8.97 (s, 1H), 11.97 (s, 1H); ¹³C NMR (101 MHz, CDCl₃): δ = 24.1 (d, *J* = 5.2 Hz), 28.1 (d, *J* = 20.1 Hz), 41.8, 83.8 (d, *J* = 165.1 Hz), 115.1, 115.8 (d, ²*J* = 22.4 Hz, 2C), 119.5, 122.3 (d, *J* = 7.8 Hz, 2C), 122.9, 134.4, 138.8, 142.8, 149.9, 152.7, 158.4, 160.8, 162.9; ¹⁹F NMR (282 MHz, CDCl₃): δ = -117.9, 11.7; HRMS (ESI⁺) *m/z* for C₁₉H₁₇F₂N₃NaO₂⁺ [M+Na]⁺ 380.1180, calcd 380.1181.

1-(4-Fluorobutyl)-2-oxo-N-(pyridin-4-yl)-1,2-dihydro-1,8-naphthyridine-3-carboxamide (24) General procedure 2, white solid in 21% yield; ¹H NMR (400 MHz, CDCl₃): δ = 1.89 (m, 4H), 4.54 (dt, *J* = 47.6, 5.8 Hz, 2H), 4.70 (t, *J* = 7.3 Hz, 2H), 7.35 (dd, *J* = 7.8, 4.7 Hz, 1H), 7.71 (d, *J* = 5.2 Hz, 2H), 8.14 (dd, *J* = 7.8, 1.9 Hz, 1H), 8.56 (s, 2H), 8.78 (dd, *J* = 4.6, 1.9 Hz, 1H), 8.98 (s, 1H), 12.24 (s, 1H); ¹³C NMR (101 MHz, CDCl₃): δ = 24.1 (d, *J* = 5.0 Hz), 28.1 (d, *J* = 20.1 Hz), 41.9, 83.8 (d, *J* = 165.2 Hz), 114.7 (s, 2C), 115.0, 119.7, 122.3, 139.0, 143.6, 145.1 (s, 2C), 150.0, 150.9, 153.1, 161.8, 162.8; ¹⁹F NMR (377 MHz, CDCl₃): δ = 218.3; HRMS (ESI⁺) *m/z* for C₁₈H₁₈FN₄O₂⁺ [M+H]⁺ 341.1420, calcd 341.1408.

N-(4-Fluorobenzyl)-1-(4-fluorobutyl)-2-oxo-1,2-dihydro-1,8-naphthyridine-3-carboxamide (25) General procedure 2, white solid in 65% yield; ¹H NMR (400 MHz, CDCl₃): δ = 1.85 (m, 4H), 4.51 (dt, *J* = 47.6, 5.7 Hz, 2H), 4.63 (dd, *J* = 9.2, 6.1 Hz, 4H), 7.03 (m, 2H), 7.30 (dd, *J* = 7.7, 4.6 Hz, 1H), 7.36 (m, 2H), 8.09 (dd, *J* = 7.8, 1.8 Hz, 1H), 8.72 (dd, *J* = 4.7, 1.6 Hz, 1H), 8.91 (s, 1H), 10.15 (s, 1H); ¹³C NMR (101 MHz, CDCl₃): δ = 24.1 (d, *J* = 5.3 Hz), 28.1 (d, *J* = 20.0 Hz), 41.6, 43.2, 83.8 (d, *J* = 165.2 Hz), 115.1, 115.6 (d, *J* = 21.5 Hz, 2C), 119.3, 122.9, 129.6 (d, *J* = 8.1 Hz, 2C), 134.3, 138.8, 142.5, 149.8, 152.4, 161.1, 162.7, 163.3 (d, *J* = 35.5 Hz); ¹⁹F NMR (377 MHz, CDCl₃): δ = -218.3, -115.5; HRMS (ESI⁺) *m/z* for C₂₀H₁₉F₂N₃NaO₂⁺ [M+Na]⁺ 394.1342, calcd 394.1338.

1-(4-Fluorobutyl)-N-(6-fluoropyridin-3-yl)-2-oxo-1,2-dihydro-1,8-naphthyridine-3-carboxamide (26) General procedure 2, white solid in 44% yield; ¹H NMR (400 MHz, CDCl₃): δ = 1.91 (m, 4H), 4.54 (dt, *J* = 47.5, 5.7 Hz, 2H), 4.71 (t, *J* = 7.3 Hz, 2H), 6.96 (m, 1H), 7.35 (dd, *J* = 7.8, 4.6 Hz, 1H), 8.15 (dd, *J* = 7.8, 1.9 Hz, 1H), 8.39 (ddd, *J* = 8.8, 7.0, 2.8 Hz, 1H), 8.53 (dd, *J* = 2.9, 1.3 Hz, 1H), 8.78 (dd, *J* = 4.7, 1.8 Hz, 1H), 8.98 (s, 1H), 12.17 (s, 1H); ¹³C NMR (101 MHz, CDCl₃): δ = 24.2 (d, *J* = 5.1 Hz), 28.1 (d,

$J = 20.1$ Hz), 41.9, 83.8 (d, $J = 165.2$ Hz), 109.6 (d, $J = 38.6$ Hz), 115.1, 119.7, 122.3, 133.1 (d, $J = 4.5$ Hz), 133.5 (d, $J = 7.5$ Hz), 139.0, 139.3 (d, $J = 15.0$ Hz), 143.2, 149.9, 153.0, 158.8, 161.3 (s, $J = 18.4$ Hz), 162.9; ^{19}F NMR (377 MHz, CDCl_3): $\delta = -218.3, -72.7$; HRMS (ESI⁺) m/z for $\text{C}_{18}\text{H}_{16}\text{F}_2\text{N}_4\text{NaO}_2^+ [\text{M}+\text{Na}]^+$ 381.1126, calcd 381.1134.

1-(4-Fluorobutyl)-2-oxo-N-(pyridin-3-yl)-1,2-dihydro-1,8-naphthyridine-3-carboxamide (27) General procedure 2, white solid in 80% yield; ^1H NMR (400 MHz, CDCl_3): $\delta = 1.91$ (m, 4H), 4.54 (dt, $J = 47.6, 5.7$ Hz, 2H), 4.71 (t, $J = 7.4$ Hz, 2H), 7.33 (dd, $J = 7.8, 4.7$ Hz, 2H), 8.14 (dd, $J = 7.8, 1.9$ Hz, 1H), 8.33 (ddd, $J = 8.4, 2.6, 1.4$ Hz, 1H), 8.40 (s, 1H), 8.76 (dd, $J = 4.7, 1.9$ Hz, 1H), 8.89 (s, 1H), 8.98 (s, 1H), 12.13 (s, 1H); ^{13}C NMR (101 MHz, CDCl_3): $\delta = 24.1$ (d, $J = 5.2$ Hz), 28.1 (d, $J = 20.1$ Hz), 41.9, 83.8 (d, $J = 165.2$ Hz), 115.0, 119.6, 122.5, 127.7, 138.9, 142.3, 143.1, 145.5, 150.0, 153.0, 161.5, 162.9; ^{19}F NMR (377 MHz, CDCl_3): $\delta = -218.3$; HRMS (ESI⁺) m/z for $\text{C}_{18}\text{H}_{18}\text{FN}_4\text{O}_2^+ [\text{M}+\text{H}]^+$ 341.1450, calcd 341.1408.

N-(Adamantan-1-yl)-1-(4-fluorobutyl)-2-oxo-1,2-dihydro-1,8-naphthyridine-3-carboxamide (28, LUI3) General procedure 2, as white solid in 81% yield; ^1H NMR (300 MHz, CDCl_3): $\delta = 1.80$ (m, 9H), 2.13 (m, 4H), 2.18 (m, 6H), 4.54 (dt, $J = 47.3, 5.8$ Hz, 2H), 4.63 (t, $J = 7.3$ Hz, 2H), 7.28 (dd, $J = 7.9, 4.6$ Hz, 1H), 8.07 (dd, $J = 7.8, 1.9$ Hz, 1H), 8.70 (dd, $J = 4.7, 1.8$ Hz, 1H), 8.84 (s, 1H), 9.64 (s, 1H); ^{13}C NMR (101 MHz, CDCl_3): $\delta = 24.1$ (d, $J = 5.4$ Hz), 28.1 (d, $J = 20.0$ Hz), 29.7, 36.6, 41.5, 41.5, 52.2, 83.9 (d, $J = 164.9$ Hz), 115.2, 119.2, 124.2, 138.7, 141.6, 149.7, 151.9, 161.4, 162.8; ^{19}F NMR (377 MHz, CDCl_3): $\delta = -218.2$; HRMS (ESI⁺) m/z for $\text{C}_{23}\text{H}_{28}\text{FN}_3\text{NaO}_2^+ [\text{M}+\text{Na}]^+$ 420.2055, calcd 420.2058.

N-(Adamantan-1-yl)-1-(4-fluorobenzyl)-2-oxo-1,2-dihydro-1,8-naphthyridine-3-carboxamide (29) General procedure 1, white solid, 73.4% yield, ^1H NMR (400 MHz, CDCl_3) δ 9.57 (s, 1H), 8.84 (s, 1H), 8.68 (d, 1H), 8.04 (d, 1H), 7.45 (m, 2H), 7.28 (m, 2H), 6.95 (m, 2H), 5.76 (s, 2H), 2.14 (m, 9H), 1.72 (m, 6H). ^{13}C NMR (75 MHz, CDCl_3) δ 164.10, 163.07, 161.49, 160.84, 152.20, 150.08, 142.04, 138.81, 133.18, 130.75, 124.67, 119.59, 115.68, 115.40, 52.41, 44.32, 41.85, 36.85, 29.85. HRMS (ESI⁺) $m/z = 432.2098$, calculated 432.2080 for $\text{C}_{26}\text{H}_{27}\text{FN}_3\text{O}_2^+ [\text{M}+\text{H}]^+$

N-(Adamantan-1-yl)-1-(2-(2-fluoroethoxy)ethyl)-2-oxo-1,2-dihydro-1,8-naphthyridine-3-carboxamide (30) NaH (60% in mineral oil, 2 equiv) was added to a solution of alcohol **49** (1 equiv) in THF (0.5 mL for 1 mmol of starting material), and the mixture was stirred for 15 min at rt. Thereafter, the alkylating agent, 2-fluoroethyl bromide, (5 equiv) was added, and the reaction mixture was stirred overnight at rt. The reaction was quenched by the addition of H_2O (2 mL), followed by 15 mL of an aqueous saturated solution of NaHCO_3 and 20 mL of CH_2Cl_2 while stirring. The phases were separated; the organic phase was washed with 20 mL of CH_2Cl_2 , and the combined organic fractions were dried over MgSO_4 and concentrated under reduced pressure. The resulting residue was subjected to column chromatography purification (silica, EA:PE, 2:3 to 3:2). The product was obtained as white solid, 2.6% yield. ^1H NMR (400 MHz, CDCl_3) δ 9.58 (s, 1H), 8.82 (s, 1H), 8.69 (m, 1H), 8.05 (m, 1H), 7.27 (m, 1H), 4.87 (t, 2H), 4.48 (m, 2H), 3.88 (t, 2H), 3.81 and 3.74 (dt, 2H), 2.14 (m, 9H), 1.72 (m, 6H). HRMS (ESI⁺) $m/z = 414.2178$, calculated 414.2176 for $\text{C}_{23}\text{H}_{29}\text{FN}_3\text{O}_3^+ [\text{M}+\text{H}]^+$

N-(Adamantan-1-yl)-1-(4-bromobutyl)-2-oxo-1,2-dihydro-1,8-naphthyridine-3-carboxamide (31B) General procedure 2, as white solid in 65% yield; ^1H NMR (400 MHz, CDCl_3) δ 9.62 (s, 1H), 8.83 (s, 1H), 8.70 (dd, $J = 4.7, 1.9$ Hz, 1H), 8.05 (dd, $J = 7.8, 1.8$ Hz, 1H), 7.32 (m, 1H), 4.62 (m, 2H), 3.49 (t, $J = 6.6$ Hz, 2H), 2.16 (m, 9H), 2.96 (m, 4H), 1.75 (m, 6H); ^{13}C NMR (101 MHz, CDCl_3): $\delta = 25.2, 29.3, 31.8, 37.0, 41.7, 41.5, 52.8, 83.6, 115.6, 118.7, 124.6, 139.1, 141.8, 149.8, 152.3, 162.2, 162.6$; HRMS (ESI⁺) m/z for $\text{BrC}_{23}\text{H}_{28}\text{N}_3\text{NaO}_2^+ [\text{M}+\text{H}]^+$ 458.1448, calcd 458.1443.

N-(Adamantan-1-yl)-1-(4-bromobutyl-1,1,2,2,3,3,4,4-ds)-2-oxo-1,2-dihydro-1,8-naphthyridine-3-carboxamide (31A) General procedure 2, before radiofluorination the product was purified by HPLC using Reprosil-Pur 120 C18-AQ (5 μm , 250x10 mm), 73% $\text{CH}_3\text{CN}/20$ mM $\text{NH}_4\text{OAc}_{\text{aq}}$, 4 mL/min. Compound **31A** was obtained as white solid in 58% yield; ^1H NMR (400 MHz, CDCl_3) δ 9.63 (s, 1H), 8.83 (s, 1H), 8.70 (dd, $J = 4.7, 1.9$ Hz, 1H), 8.05 (dd, $J = 7.8, 1.8$ Hz, 1H), 7.28 (m, 1H), 2.16 (m, 9H), 1.74 (m, 6H); ^{13}C NMR (101 MHz, CDCl_3): $\delta = 25.8, 28.6, 32.2, 36.8, 41.5, 41.8, 52.7, 83.5, 115.7, 118.9, 125.1, 138.7, 142.1, 149.5, 151.9, 162.3, 161.9$; HRMS (ESI⁺) m/z for $\text{BrC}_{23}\text{H}_{20}\text{D}_8\text{N}_3\text{NaO}_2^+ [\text{M}+\text{H}]^+$ 466.1948, calcd 466.1945.

Radiochemistry

Automated radiosynthesis of [^{18}F]LUI3

Remote-controlled radiosynthesis was performed using a Synchro R&D EVO III automated synthesizer (Elysia-Raytest, Germany). Briefly, [^{18}F]fluoride (4-6 GBq) was loaded on a pre-conditioned (15 mL 0.5 M NaHCO_3 and 10 mL H_2O) Sep-Pak[®] Accell Plus QMA Carbonate Plus Light cartridge (Waters GmbH; Eschborn; Germany) and eluted with a solution containing 100 μL TBAHCO₃ (0.5 M) and 46 μL K_2CO_3 (20 g/L) dissolved in a mixture of $\text{H}_2\text{O}/\text{CH}_3\text{CN}$ (1 mL, 1:4, v/v) into the reaction vessel and dried via azeotropic distillation. Additional 1.5 mL of dried CH_3CN was added. After complete dryness, a solution containing 2 mg of precursor **31** in 800 μL DMSO was added, and the reaction mixture was stirred at 120 °C for 10 min. The reaction mixture was cooled to 40 °C, diluted with 4 mL H_2O and transferred into the injection vial for isolation of the radiotracer by preparative HPLC. First, [^{18}F]LUI3 was collected in the HPLC collection vial containing 40 mL of H_2O and then trapped on a pre-conditioned (5 mL EtOH and 30 mL H_2O) RP-cartridge (Sep-Pak[®] C18 Light; Waters GmbH; Eschborn; Germany). The cartridge was washed with 2 mL H_2O , and [^{18}F]LUI3 was eluted with 1.2 mL EtOH. This ethanolic solution was transferred outside of the shielded cell, the solvent was reduced at 70 °C in a gentle stream of nitrogen for 5-10 min to a volume of about 20-30 μL , and [^{18}F]LUI3 was formulated in 280 μL isotonic saline solution up to a final concentration of < 10% EtOH for further biological characterization. The total synthesis time was about 80 min.

Quality control

Radio-TLC was performed on Alugram[®] SIL G/UV₂₅₄ pre-coated plates (Macherey-Nagel; Düren, Germany) with PE:EA (1:1, v/v). The plates were exposed to storage phosphor screens (BAS IP MS 2025 E, GE Healthcare Europe GmbH, Freiburg, Germany) and recorded using the Amersham Typhoon RGB Biomolecular Imager (GE Healthcare Life Sciences). Images were quantified with the ImageQuant TL8.1 software (GE Healthcare Life Sciences).

Analytical chromatographic separations were performed on a JASCO LC-2000 system, incorporating a PU-2080Plus pump, AS-2055Plus auto injector (100 μL sample loop), and a UV-2070Plus detector coupled with a γ -detector (GABI Star; raytest Isoto-15

penmessgeräte GmbH, Straubenhardt, Germany). Data analysis was performed with the Galaxie chromatography software (Agilent Technologies, Santa Clara, CA, USA) using chromatograms obtained at 254 nm.

Radiochemical yield, radiochemical purity, and analyses of plasma and brain samples were assessed via reversed-phase HPLC (RP-HPLC) in gradient mode (0–10 min: 10% CH₃CN/20 mM NH₄OAc_{aq}, 10–30 min: 10%→90% CH₃CN/20 mM NH₄OAc_{aq}, 30–35 min: 90% CH₃CN/20 mM NH₄OAc_{aq}, 35–36 min: 90%→10% CH₃CN/20 mM NH₄OAc_{aq}, 36–45 min: 10% CH₃CN/20 mM NH₄OAc_{aq}).

Molar activities were determined based on aliquots taken from the formulation, and the mass determination for the corresponding reference standard was performed via a calibration curve (0.5–0.015 µg **LU13**; isocratic conditions: 62% CH₃CN/20 mM NH₄OAc_{aq}; analytical Reprosil-Pur 120 C18-AQ column) using chromatograms obtained at 224 nm as the maximum of UV absorbance.

Biological experiments

All studies involving animals were carried out according to the national laws on the protection of animals and were approved by the responsible authorities (Landesdirektion Sachsen, Reference No. DD24.1-5131/446/19, TVV 18/18).

Determination of binding affinities by homogenate assays

The binding affinities towards hCB1R and hCB2R were determined according to a previously published protocol.³⁹ In brief, membrane preparations obtained from CHO cell lines stably transfected with either human CB1R (hCB1R-CHO; obtained from Euroscreen, Gosselies, Belgium) or human CB2R (hCB2R-CHO; obtained from Paul L. Prather, Department of Pharmacology and Toxicology, College of Medicine, University of Arkansas for Medical Sciences, USA) were incubated with [³H]SR141716A (1,554 GBq/mmol; PerkinElmer Life and Analytical Sciences, Rodgau, Germany; final concentration ~ 2 nM) or [³H]WIN55212-2 (6,438 GBq/mmol; PerkinElmer Life and Analytical Sciences, Rodgau, Germany; final concentration ~ 3 nM) and the respective test compounds at different concentrations (final concentration 10⁻⁵ M–10⁻¹¹ M) diluted from DMSO stock solutions (1% DMSO final concentration) in incubation buffer (50 mM TRIS-HCl, pH 7.4, supplemented with 0.1% bovine serum albumin, 5 mM MgCl₂, and 1 mM EDTA) at rt for 90 min.

Homologous radioligand displacement studies investigating the potential of **LU13** to displace [¹⁸F]**LU13** from binding sites in membrane homogenates of rat spleen or hCB2R-CHO cells were performed according to the same protocol.

The non-specific binding of the respective radioligand was determined by co-incubation with CP55,940 (final concentration 10⁻⁵ M). The normalized values of bound activity (% specific binding) were calculated and plotted vs. the logarithm of the concentration of the respective test compound. The IC₅₀ values of the resulting inhibition curves were estimated by nonlinear regression analysis (GraphPad Prism 2.01). To calculate the K_i, the equation of Cheng and Prusoff was used. For homologous competition experiments, K_i = K_D.⁵⁹

Quantification of radiometabolites

About 30 MBq [¹⁸F]**LU13** dissolved in about 150 µL isotonic saline was administered as a bolus in the tail vein of temporarily restrained non-anesthetized female CD-1 mice weighing about 33 g (n = 3). At 30 min p.i., the animals were anesthetized by isoflurane inhalation and blood was withdrawn by retro-orbital bleeding from the venous sinus. Immediately afterwards, the anesthetized animals were euthanized by cervical dislocation, and the released urine was sampled. Blood plasma was obtained from the whole blood sample by centrifugation (2 min, 8000 rpm, rt). In addition, the brain and spleen were isolated and homogenized in 1 ml demineralised water on ice (1000 rpm, 10 strokes; glass vessel, PTFE plunger; Potter S, B. Braun Biotech International, Göttingen, Germany).

The samples were further processed for subsequent radio-chromatographic analyses. Two consecutive extractions were performed as duplicates for plasma and brain determinations. Plasma, brain and spleen samples were added to an ice-cold MeOH/H₂O mixture (9:1, v/v). The samples were vortexed for 3 min, incubated on ice for 5 min and centrifuged at 10,000 rpm for 5 min. Supernatants were collected and the precipitates were re-dissolved in 100 µL of extraction solvent and the extraction procedure was repeated. The activities of supernatants and precipitates were measured in a γ-counter (1480 WIZARD, Perkin Elmer), and the extraction efficiencies were calculated as ratio of radioactivity in the supernatant to the radioactivity in the original sample (supernatant + precipitate). The supernatants from both extractions were combined, concentrated at 70 °C under argon stream up to a remaining volume of 100 µL, and subsequently analysed by analytical radio-HPLC with a gradient system (see quality control section).

PET studies

In vivo brain uptake of [¹⁸F]**LU13** in rats was assessed by dynamic small animal PET (Nanoscan, Mediso, Budapest, Hungary) 60 min recordings, followed by T1-weighted (GRE, TR/TE=15.0/2.4 ms, 252/252, FA=25°) MR imaging with whole-body coils for anatomical correlation and attenuation correction. For the uptake studies into the brain, five female Wistar rats weighing 280 ± 5 g carrying the stereotactically injected AAV 2/7-CaMKII0.4-intron-hCB2R D80N (right striatum) and AAV2/7-CaMKII0.4-intron-3flag-eGFP (control, left striatum) were used. The PET scans were performed seven months after the stereotactic injections. Displacement studies were performed with three randomly chosen animals seven days after the PET study injecting the vehicle. Animals were initially anaesthetized with 5% isoflurane and placed on a thermostatically heated animal bed where anaesthesia was maintained with 2% isoflurane in 60% oxygen/38% room air. They were pre-treated either by i.v. injections of vehicle solution only, containing DMSO : Kolliphor EL : saline in a composition of 1 : 2 : 7 (control group) or 5 mg/kg GW405833 for the displacement experiments 20 minutes after [¹⁸F]**LU13** administration. [¹⁸F]**LU13** (21 to 28 MBq, ~20 pmol) was injected into the lateral tail vein (bolus within 5 s) at the start of the PET acquisition. List-mode PET data were binned as a series of attenuation-corrected sinogram frames (12 × 10 s, 6 × 30 s, 5 × 60 s and 10 × 300 s) and were reconstructed by ordered subset expectation maximization (OSEM3D) with four iterations, six subsets and a voxel size of 0.4 mm³ (Nucline v2.01, Mediso, Hungary). The analysis of reconstructed datasets was performed with PMOD software (v4.103, PMOD Technologies LLC, Zurich, Switzerland). Non-parametrical analysis of achieved time-activity curves (TACs) were performed with Microsoft Excel to determine the time to peak, the TAC

peak value, the area-under the curve (AUC):

$$AUC_{0-t(x)} = \int_0^{t(x)} c(\text{radioactivity}) \times dt$$

where c (radioactivity) is expressed as standardized uptake value normalized to the bodyweight in g (SUV), the area-under-the-moment curve (AUMC):

$$AUMC_{0-t(x)} = \int_0^{t(x)} t \times c(\text{radioactivity}) \times dt, \quad (2)$$

and the mean residence time (MRT):

$$MRT = \frac{AUMC_{0-t(x)}}{AUC_{0-t(x)}} \quad (3)$$

Data are shown in mean \pm standard deviation (SD). Group differences were tested by Student's t-test, with $p < 0.05$ designated as significant. Area Under the Curves (AUCs) and corresponding 95% confidence intervals (CI, 95%) were calculated with GraphPad Prism (v.8.2) following the assumptions described by Gagnon et al.⁶⁰

ASSOCIATED CONTENT

Supporting Information

NMR characterization of compounds **10-16** and 20-31; In vitro rat spleen autoradiography of [¹⁸F]LU13 (Figure S1); Time activity curves of the contralateral site and the cerebellum, with and without (vehicle) GW405833 (5mg/Kg, n = 3) administered at 20 min post injection of [¹⁸F]LU13 and the corresponding AUCs (n = 3; Mean \pm SD) (Figure S2); Molecular Formula Strings for all target compounds.

Corresponding Author

* Rareş-Petru Moldovan (r.moldovan@hzdr.de, Tel.: +49-3412341794634)

Author Contributions

The manuscript was written through contributions of all authors. / All authors have given approval to the final version of the manuscript.

Funding Sources

This research was funded by Deutsche Forschungsgemeinschaft (DFG), grant number MO2677/4-1

ACKNOWLEDGMENT

We would like to thank the staff of the Institute of Analytical Chemistry, Department of Chemistry and Mineralogy of Universität Leipzig (Leipzig; Germany), for NMR and HRFT-MS measurements, Dr. Karsten Franke, Helmholtz-Zentrum Dresden-Rossendorf (HZDR) for providing [¹⁸F]fluoride as well as Mrs. Tina Spalholz, HZDR, for her support in the cultivation of cells and for performing the binding assays with the ³H-labeled radioligands.

ABBREVIATIONS

BOP, (benzotriazol-1-yloxy)tris-(dimethylamino)phosphonium hexafluorophosphate; BBB, blood-brain barrier; CB1R, cannabinoid receptors type 1; CB2R, cannabinoid receptors type 2; K_{2.2.2}, 2.2.2-Cryptand; DMF, N,N-dimethylformamide; HPLC, high-performance liquid chromatography; PET, positron emission tomography; p.i., post injection; LPS, lipopolysaccharide; SAR, structure-activity relationship; SUV, standardized uptake value; SUVr, SUV ratio x-to-reference; TBAF, tetrabutylammonium fluoride; THC, (-)-trans- Δ^9 -tetrahydrocannabinol; Et₃N, triethylamine.

REFERENCES

1. Baker, D.; Pryce, G.; Giovannoni, G.; Thompson, A. J., The therapeutic potential of cannabis. *Lancet. Neurol.* **2003**, 2 (5), 291-298.
2. Reggio, P. H., Endocannabinoid binding to the cannabinoid receptors: What is known and what remains unknown. *Curr. Med. Chem.* **2010**, 17 (14), 1468-1486.
3. Rimplejeet, K.; Sneha, R. A.; Surjit, S., Endocannabinoid system: A multi-facet therapeutic target. *Curr. Clin. Pharmacol.* **2016**, 11 (2), 110-117.
4. Russo, E. B., Beyond cannabis: plants and the endocannabinoid system. *Trends Pharmacol. Sci.* **2016**, 37 (7), 594-605.
5. Matsuda, L. A.; Lolait, S. J.; Brownstein, M. J.; Young, A. C.; Bonner, T. I., Structure of a cannabinoid receptor and functional

- expression of the cloned cDNA. *Nature* **1990**, *346* (6284), 561-564.
6. Munro, S.; Thomas, K. L.; Abu-Shaar, M., Molecular characterization of a peripheral receptor for cannabinoids. *Nature* **1993**, *365* (6441), 61-65.
 7. Latek, D.; Kolinski, M.; Ghoshdastider, U.; Debinski, A.; Bombolewski, R.; Plazinska, A.; Jozwiak, K.; Filipek, S., Modeling of ligand binding to G protein coupled receptors: cannabinoid CB1, CB2 and adrenergic β 2AR. *J. Mol. Mod.* **2011**, *17* (9), 2353-2366.
 8. Vendel, E.; de Lange, E. C., Functions of the CB₁ and CB₂ receptors in neuroprotection at the level of the blood-brain barrier. *Neuromolecular. Med.* **2014**, *16* (3), 620-42.
 9. Silvestri, C.; Di Marzo, V., The endocannabinoid system in energy homeostasis and the etiopathology of metabolic disorders. *Cell Metabol.* **2013**, *17* (4), 475-490.
 10. Malan, T. P., Jr.; Ibrahim, M. M.; Lai, J.; Vanderah, T. W.; Makriyannis, A.; Porreca, F., CB₂ cannabinoid receptor agonists: pain relief without psychoactive effects? *Curr. Opin. Pharmacol.* **2003**, *3* (1), 62-7.
 11. Ashton, J. C.; Friberg, D.; Darlington, C. L.; Smith, P. F., Expression of the cannabinoid CB₂ receptor in the rat cerebellum: An immunohistochemical study. *Neurosci. Lett.* **2006**, *396* (2), 113-116.
 12. Chen, D. J.; Gao, M.; Gao, F. F.; Su, Q. X.; Wu, J., Brain cannabinoid receptor 2: Expression, function and modulation. *Acta Pharmacol. Sin.* **2017**, *38* (3), 312-316.
 13. Komorowska-Müller, J. A.; Schmöle, A.-C., CB₂ receptor in microglia: The guardian of self-control. *Int. J. Mol. Sci.* **2021**, *22* (1), 19.
 14. Roche, M.; Finn, D. P., Brain CB₂ receptors: Implications for neuropsychiatric disorders. *Pharmaceuticals* **2010**, *3* (8), 2517-2553.
 15. Lin, L.; Yihao, T.; Zhou, F.; Yin, N.; Qiang, T.; Haowen, Z.; Qianwei, C.; Jun, T.; Yuan, Z.; Gang, Z.; Hua, F.; Yunfeng, Y.; Zhi, C., Inflammatory regulation by driving microglial M2 polarization: Neuroprotective effects of cannabinoid receptor-2 activation in intracerebral hemorrhage. *Front. Immunol.* **2017**, *8*, 112-112.
 16. Tao, Y.; Li, L.; Jiang, B.; Feng, Z.; Yang, L.; Tang, J.; Chen, Q.; Zhang, J.; Tan, Q.; Feng, H.; Chen, Z.; Zhu, G., Cannabinoid receptor-2 stimulation suppresses neuroinflammation by regulating microglial M1/M2 polarization through the cAMP/PKA pathway in an experimental GMH rat model. *Brain, Behav. Immun.* **2016**, *58*, 118-129.
 17. Tanaka, M.; Sackett, S.; Zhang, Y., Endocannabinoid modulation of microglial phenotypes in neuropathology. *Front. Neurol.* **2020**, *11*.
 18. Benito, C.; Tolón, R. M.; Pazos, M. R., Cannabinoid CB₂ receptors in human brain inflammation. *Br. J. Pharmacol.* **2008**, *153*.
 19. Benito, C.; Núñez, E.; Tolón, R. M.; Carrier, E. J.; Rábano, A.; Hillard, C. J.; Romero, J., Cannabinoid CB₂ receptors and fatty acid amide hydrolase are selectively overexpressed in neuritic plaque-associated glia in alzheimer's disease brains. *J. Neurosci.* **2003**, *23* (35), 11136-11141.
 20. Casteels, C.; Ahmad, R.; Vandenbulcke, M.; Vandenbergh, W.; Van Laere, K., Chapter 4 - Cannabinoids and Huntington's disease. In *Cannabinoids in neurologic and mental disease*, Academic Press: San Diego, 2015; pp 61-97.
 21. Fernandez-Ruiz, J.; Romero, J.; Ramos, J. A., Endocannabinoids and neurodegenerative disorders: Parkinson's Disease, Huntington's Chorea, Alzheimer's Disease, and others. *Handb. Exp. Pharmacol.* **2015**, *231*, 233-259.
 22. Bisogno, T.; Oddi, S.; Piccoli, A.; Fazio, D.; Maccarrone, M., Type-2 cannabinoid receptors in neurodegeneration. *Pharmacol. Res.* **2016**, *111*, 721-730.
 23. Palazuelos, J.; Aguado, T.; Pazos, M. R.; Julien, B.; Carrasco, C.; Resel, E.; Sagredo, O.; Benito, C.; Romero, J.; Azcoitia, I.; Fernández-Ruiz, J.; Guzmán, M.; Galve-Roperh, I., Microglial CB₂ cannabinoid receptors are neuroprotective in Huntington's disease excitotoxicity. *Brain* **2009**, *132* (11), 3152-3164.
 24. Di Iorio, G.; Lupi, M.; Sarchione, F.; Matarazzo, I.; Santacroce, R.; Petrucci, F.; Martinotti, G.; Di Giannantonio, M., The endocannabinoid system: a putative role in neurodegenerative diseases. *Int. J. High. Risk. Behav. Addict.* **2013**, *2* (3), 100-106.
 25. Yiangou, Y. F., P.; Banati, R. B.; O'Shaughnessy, C. T.; Chessell, I. P.; Anand, P., Cannabinoid receptor CB₂ expression in activated microglia of multiple sclerosis and amyotrophic lateral sclerosis spinal cord. *J. Neurol. Neurosurg. Psychiatry* **2004**, *75* (8), 1228.
 26. Kucerova, J.; Tabiova, K.; Drago, F.; Micale, V., Therapeutic potential of cannabinoids in schizophrenia. *Recent Pat. CNS Drug. Discov.* **2014**, *9* (1), 13-25.
 27. Ellert-Miklaszewska, A.; Ciechomska, I.; Kaminska, B., Cannabinoid signaling in glioma cells. *Adv. Exp. Med. Biol.* **2013**, *986*, 209-220.
 28. Jia, N.; Zhang, S.; Shao, P.; Bagia, C.; Janjic, J. M.; Ding, Y.; Bai, M., Cannabinoid CB₂ receptor as a new phototherapy target for the inhibition of tumor growth. *Mol. Pharm.* **2014**, *11* (6), 1919-1929.
 29. Nikan, M.; Nabavi, S. M.; Manayi, A., Ligands for cannabinoid receptors, promising anticancer agents. *Life Sci.* **2016**, *146*, 124-30.
 30. Sarfaraz, S.; Adhami, V. M.; Syed, D. N.; Afaq, F.; Mukhtar, H., Cannabinoids for cancer treatment: progress and promise. *Cancer Res.* **2008**, *68* (2), 339-342.
 31. Meccariello, R., Endocannabinoid system in health and disease: Current situation and future perspectives. *Int. J. Molecul. Sci.* **2020**, *21* (10), 3549.
 32. Cabañero, D.; Martín-García, E.; Maldonado, R., The CB₂ cannabinoid receptor as a therapeutic target in the central nervous system. *Expert Opin. Ther. Targets* **2021**, *25* (8), 659-676.
 33. Hou, L.; Rong, J.; Haider, A.; Ogasawara, D.; Varlow, C.; Schafroth, M. A.; Mu, L.; Gan, J.; Xu, H.; Fowler, C. J.; Zhang, M.-R.; Vasdev, N.; Ametamey, S.; Cravatt, B. F.; Wang, L.; Liang, S. H., Positron emission tomography imaging of the endocannabinoid system: Opportunities and challenges in radiotracer development. *J. Med. Chem.* **2021**, *64* (1), 123-149.
 34. Terry, G. E.; Raymond, V.; Horti, A. G., PET imaging of the endocannabinoid system. In *PET and SPECT of Neurobiological Systems*, Dierckx, R. A. J. O.; Otte, A.; de Vries, E. F. J.; van Waarde, A.; Lammertsma, A. A., Eds. Springer International Publishing: Cham, 2021; pp 319-426.
 35. Ni, R.; Mu, L.; Ametamey, S., Positron emission tomography of type 2 cannabinoid receptors for detecting inflammation in the central nervous system. *Acta Pharmacol. Sin.* **2019**, *40* (3), 351-357.

36. Evens, N.; Vandeputte, C.; Coolen, C., Preclinical evaluation of [¹¹C]NE40, a type 2 cannabinoid receptor PET tracer. *Nuc. Med. Biol.* **2012**, *39* (3), 389-399.
37. Postnov, A.; Ahmad, R.; Evens, N., Quantification of [¹¹C]NE40, a novel PET radioligand for CB2 receptor imaging. *J. Nucl. Med.* **2013**, *54* ((supplement 2)), 188.
38. Ahmad, R.; Postnov, A.; Bormans, G.; Versijpt, J.; Vandenbulcke, M.; Van Laere, K., Decreased *in vivo* availability of the cannabinoid type 2 receptor in Alzheimer's disease. *Eur. J. Nucl. Med. Mol. Imaging.* **2016**, *43* (12), 2219-2227.
39. Moldovan, R.-P.; Teodoro, R.; Gao, Y.; Deuther-Conrad, W.; Kranz, M.; Wang, Y.; Kuwabara, H.; Nakano, M.; Valentine, H.; Fischer, S.; Pomper, M. G.; Wong, D. F.; Dannals, R. F.; Brust, P.; Horti, A. G., Development of a high-affinity PET radioligand for imaging cannabinoid subtype 2 receptor. *J. Med. Chem.* **2016**, *59* (17), 7840-7855.
40. Moldovan, R.-P.; Deuther-Conrad, W.; Teodoro, R.; Wang, Y.; Fischer, S.; Pomper, M.; Wong, D.; Dannals, R.; Brust, P.; Horti, A., [¹⁸F]JHU94620, a high affinity PET radioligand for imaging of cannabinoid subtype 2 receptors (CB2R). *J. Nucl. Med.* **2015**, *56* (supplement 3), 1048.
41. Mu, L.; Bieri, D.; Slavik, R.; Drandarov, K.; Muller, A.; Cermak, S.; Weber, M.; Schibli, R.; Kramer, S. D.; Ametamey, S. M., Radiolabeling and *in vitro/in vivo* evaluation of *N*-(1-adamantyl)-8-methoxy-4-oxo-1-phenyl-1,4-dihydroquinoline-3-carboxamide as a PET probe for imaging cannabinoid type 2 receptor. *J. Neurochem.* **2013**, *126* (5), 616-624.
42. Mu, L.; Slavik, R.; Muller, A.; Popaj, K.; Cermak, S.; Weber, M.; Schibli, R.; Kramer, S. D.; Ametamey, S. M., Synthesis and preliminary evaluation of a 2-oxoquinoline carboxylic acid derivative for PET imaging the cannabinoid type 2 receptor. *Pharmaceuticals* **2014**, *7* (3), 339-352.
43. Slavik, R.; Herde, A. M.; Bieri, D.; Weber, M.; Schibli, R.; Kramer, S. D.; Ametamey, S. M.; Mu, L., Synthesis, radiolabeling and evaluation of novel 4-oxo-quinoline derivatives as PET tracers for imaging cannabinoid type 2 receptor. *Eur. J. Med. Chem.* **2015**, *92c*, 554-564.
44. Haider, A.; Gobbi, L.; Kretz, J.; Ullmer, C.; Brink, A.; Honer, M.; Woltering, T. J.; Muri, D.; Iding, H.; Bürkler, M.; Binder, M.; Bartelmus, C.; Knuesel, L.; Pacher, P.; Herde, A. M.; Spinelli, F.; Ahmed, H.; Atz, K.; Keller, C.; Weber, M.; Schibli, R.; Mu, L.; Grether, U.; Ametamey, S. M., Identification and preclinical development of a 2,5,6-trisubstituted fluorinated pyridine derivative as a radioligand for the positron emission tomography imaging of cannabinoid type 2 receptors. *J. Med. Chem.* **2020**, *63* (18), 10287-10306.
45. Ni, R.; Müller Herde, A.; Haider, A.; Keller, C.; Louloudis, G.; Vaas, M.; Schibli, R.; Ametamey, S. M.; Klohs, J.; Mu, L., *In vivo* imaging of cannabinoid type 2 receptors: Functional and structural alterations in mouse model of cerebral ischemia by PET and MRI. *Mol. Imag. Biol.* **2021**.
46. Teodoro, R.; Gündel, D.; Deuther-Conrad, W.; Ueberham, L.; Toussaint, M.; Bormans, G.; Brust, P.; Moldovan, R.-P., Development of [¹⁸F]LU14 for PET imaging of cannabinoid receptor type 2 in the brain. *Int. J. Mol. Sci.* **2021**, *22* (15), 8051.
47. Lucchesi, V.; Hurst, D. P.; Shore, D. M.; Bertini, S.; Ehrmann, B. M.; Allarà, M.; Lawrence, L.; Ligresti, A.; Minutolo, F.; Saccomanni, G.; Sharir, H.; Macchia, M.; Di Marzo, V.; Abood, M. E.; Reggio, P. H.; Manera, C., CB₂-Selective Cannabinoid Receptor Ligands: Synthesis, Pharmacological Evaluation, and Molecular Modeling Investigation of 1,8-Naphthyridin-2(1*H*)-one-3-carboxamides. *J. Med. Chem.* **2014**, *57* (21), 8777-8791.
48. Pascali, G.; Panetta, D.; De Simone, M.; Burchielli, S.; Lucchesi, V.; Sanguinetti, E.; Zanoni, S.; Iozzo, P.; Saccomanni, G.; Manera, C.; Salvadori, P. A., Preliminary investigation of a novel ¹⁸F radiopharmaceutical for imaging CB₂ receptors in a SOD mouse model. *Austr. J. Chem.* **2021**.
49. Manera, C.; Saccomanni, G.; Adinolfi, B.; Benetti, V.; Ligresti, A.; Cascio, M. G.; Tuccinardi, T.; Lucchesi, V.; Martinelli, A.; Nieri, P.; Masini, E.; Di Marzo, V.; Ferrarini, P. L., Rational design, synthesis, and pharmacological properties of new 1,8-naphthyridin-2(1*H*)-on-3-carboxamide derivatives as highly selective cannabinoid-2 receptor agonists. *J. Med. Chem.* **2009**, *52* (12), 3644-3651.
50. Kuchar, M.; Mamat, C., Methods to increase the metabolic stability of ¹⁸F-radiotracers. *Molecules* **2015**, *20* (9), 16186-16220.
51. Klenner, M. A.; Pascali, G.; Fraser, B. H.; Darwish, T. A., Kinetic isotope effects and synthetic strategies for deuterated carbon-11 and fluorine-18 labeled PET radiopharmaceuticals. *Nuc. Med. Biol.* **2021**, *96-97*, 112-147.
52. Vandeputte, C.; Evens, N.; Toelen, J.; Deroose, C. M.; Bosier, B.; Ibrahim, A.; Van der Perren, A.; Gijssbers, R.; Janssen, P.; Lambert, D. M.; Verbruggen, A.; Debyser, Z.; Bormans, G.; Baekelandt, V.; Van Laere, K., A PET brain reporter gene system based on type 2 cannabinoid receptors. *J. Nucl. Med.* **2011**, *52* (7), 1102-1109.
53. Attili, B.; Celen, S.; Ahamed, M.; Koole, M.; Haute, C. V. D.; Vanduffel, W.; Bormans, G., Preclinical evaluation of [¹⁸F]MA3: a CB₂ receptor agonist radiotracer for PET. *Brit. J. Pharmacol.* **2019**, *176* (10), 1481-1491.
54. Pajouhesh, H.; Lenz, G. R., Medicinal chemical properties of successful central nervous system drugs. *NeuroRx*. **2005**, *2* (4), 541-553.
55. Waterhouse, R. N., Determination of lipophilicity and its use as a predictor of blood-brain barrier penetration of molecular imaging agents. *Mol. Imag. Biol.* **2003**, *5* (6), 376-389.
56. Kawamoto, K.; Zhong, M.; Wang, R.; Olsen, B. D.; Johnson, J. A., Loops versus branch functionality in model click hydrogels. *Macromolecules* **2015**, *48* (24), 8980-8988.
57. Newton, P.; Harrison, P.; Clulow, S., A novel method for determination of the affinity of protein: Protein interactions in homogeneous assays. *SLAS Discovery* **2008**, *13* (7), 674-682.
58. Moldovan, R. P.; Wenzel, B.; Teodoro, R.; Neumann, W.; Dukic-Stefanovic, S.; Kraus, W.; Rong, P.; Deuther-Conrad, W.; Hey-Hawkins, E.; Krugel, U.; Brust, P., Studies towards the development of a PET radiotracer for imaging of the P2Y₁ receptors in the brain: synthesis, ¹⁸F-labeling and preliminary biological evaluation. *Eur. J. Med. Chem.* **2019**, *165*, 142-159.
59. Yung-Chi, C.; Prusoff, W. H., Relationship between the inhibition constant (*K_i*) and the concentration of inhibitor which causes 50 per cent inhibition (*I₅₀*) of an enzymatic reaction. *Biochem. Pharmacol.* **1973**, *22* (23), 3099-3108.
60. Gagnon, R. C.; Peterson, J. J., Estimation of confidence intervals for area under the curve from destructively obtained pharmacokinetic data. *J. Pharmacokinetic. Biopharm.* **1998**, *26* (1), 87-102.

Table of Contents Graphic

